PHILOSOPHICAL TRANSACTIONS OF THE ROYAL SOCIETY A

Phil. Trans. R. Soc. A (2007) **365**, 1793–1828
doi:10.1098/rsta.2007.2048
Published online 18 May 2007

Constraining past global tropospheric methane budgets with carbon and hydrogen isotope ratios in ice

By Michael Whiticar* and Hinrich Schaefer†

School of Earth and Ocean Sciences, University of Victoria, PO Box 3055, Victoria, British Columbia V8W 3P6, Canada

Upon closer inspection, the classical view of the synchronous relationship between tropospheric methane mixing ratio and Greenland temperature observed in ice samples reveals clearly discernable variations in the magnitude of this response during the Late Pleistocene (<50 kyr BP). During the Holocene this relationship appears to decouple, indicating that other factors have modulated the methane budget in the past 10 kyr BP. The $\delta^{13}CH_4$ and $\delta D\text{-}CH_4$ of tropospheric methane recorded in ice samples provide a useful constraint on the palaeomethane budget estimations. Anticipated changes in palaeoenvironmental conditions are recorded as changes in the isotope signals of the methane precursors, which are then translated into past global $\delta^{13}CH_4$ and $\delta D\text{-}CH_4$ signatures. We present the first methane budgets for the late glacial period that are constrained by dual stable isotopes. The overall isotope variations indicate that the Younger Dryas (YD) and Preindustrial Holocene have methane that is ^{13}C- and ^{2}H-enriched, relative to Modern. The shift is small for $\delta^{13}CH_4$ (approx. 1‰) but greater for $\delta D\text{-}CH_4$ (approx. 9‰). The YD $\delta^{13}CH_4$–$\delta D\text{-}CH_4$ record shows a remarkable relationship between them from 12.15 to 11.52 kyr BP. The corresponding C- and H-isotope mass balances possibly indicate fluctuating emissions of thermogenic gas. This $\delta^{13}CH_4$–$\delta D\text{-}CH_4$ relationship breaks down during the YD–Preboreal transition. In both age cases, catastrophic releases of hydrates with Archaeal isotope signatures can be ruled out. Thermogenic clathrate releases are possible during the YD period, but so are conventional natural gas seepages.

Keywords: palaeotemperatures and atmospheric methane budgets; stable carbon and hydrogen isotopes; Preindustrial Holocene; Younger Dryas; Late Glacial Maximum; Greenland ice

1. Introduction

The world is entering an unprecedented period in our history where changes to our climate are being induced by our release of radiatively active greenhouse gases (GHGs) into the atmosphere. Anthropogenic emissions of GHGs, such as CO_2,

* Author for correspondence (whiticar@uvic.ca).
† Present address: Department of Geosciences, Oregon State University, 104 Wilkinson Hall, Corvallis, OR 97331, USA.

One contribution of 18 to a Discussion Meeting Issue 'Trace gas biogeochemistry and global change'.

CH_4 and N_2O, continue to increase these tropospheric gas burdens. For example, the 5 Gt of methane in the atmosphere today raises the global temperature by approximately 1.3 K (Donner & Ramanathan 1980), and the change in forcing by methane since 1750 has been 0.55 W m^{-2} (Minschwaner *et al.* 1998; Jain *et al.* 2000). Our knowledge that these changes are occurring are founded on meticulous time-series trace gas measurements, such as the NOAA CMDL CCGG cooperative air sampling network (e.g. Conway *et al.* 1994; Dlugokencky *et al.* 2005), or the visionary Mona Lau dataset (Keeling & Whorf 2005).

Today, the global methane mixing ratio, $[CH_4]$, is 1780 ppbv (CMDL NOAA data; Dlugokencky *et al.* 1994, 2003) and is currently rising at a rate of 4 ± 4 ppbv yr^{-1} (Dlugokencky *et al.* 1998, 2005; Bousquet *et al.* 2006). Using bottom-up approaches, i.e. wide-ranging field measurements of CH_4 emissions intensities from the significant sources and relevant CH_4 sinks, we are able to generate reasonable models to describe today's atmospheric CH_4 budget. Although sizable uncertainties remain in accurately characterizing the magnitude and changes of the major types of source fluxes, the budgets can be constrained by knowledge of the tropospheric CH_4 burden, the present day stable carbon and hydrogen isotope ratios ($\delta^{13}CH_4$ and $\delta D\text{-}CH_4$, respectively) and the radiogenic $^{14}CH_4$. The increase in present day $[CH_4]$ over the natural background is largely the result of anthropogenic releases of gas from sources such as rice paddies, landfills, livestock, biomass burning and natural gas usage. The associated rise in global temperature causes serious feedbacks that exacerbate the issue. These may also involve the elevation of CH_4 emissions from natural sources, including enhanced methanogenesis from tropical and boreal wetlands, CH_4 release by retreating permafrost, and the potential destabilization of marine and terrestrial CH_4 clathrates (gas hydrates). A key component to our understanding of climate variability is to differentiate natural and anthropogenic methane emissions and sinks for present and past periods e.g. Prather *et al.* (2001) and Wunsch (2006).

The current methane concentration $[CH_4]$ represents an approximately 2.5 times increase in tropospheric methane in comparison with times before intensive human interference i.e. the Late Preindustrial Holocene (PIH; 2000 years BP), when $[CH_4]$ was approximately 700 ppbv (e.g. Etheridge *et al.* 1998; Ferretti *et al.* 2005). Further back in time, during glacial periods, $[CH_4]$ was up to five-times less than at present, i.e. $[CH_4]$ approximately 320–400 ppbv. We know this from detailed tropospheric gas histories chronologically recorded back to *ca* 650 kyr BP in the occluded bubbles of the Antarctic ice sheets (Spahni *et al.* 2005) and 110 kyr BP in the Greenland ice sheets (Brook *et al.* 1996, 2000). These time-series reveal that tropospheric methane concentrations systematically rose and fell within the range of approximately 350–750 ppbv. Over orbital cycles, the variations of $[CH_4]$ in the ice track those of other indicators, such as $[CO_2]$ and temperature (Petit *et al.* 1999). However, a detailed view shows that $[CH_4]$ is very closely correlated with Greenland temperature, which is antiphased with Antarctic climate throughout the last glacial period. For the end of the last ice age, the gas stratigraphy of the Greenland GISP2 cores, as established with thermally fractionated nitrogen and noble gas isotopes, suggests that the rapid rises in Greenland temperature lead the corresponding rises in $[CH_4]$ by up to 50 years (Severinghaus *et al.* 1998; Severinghaus & Brook 1999). In comparison, the rises in $[CO_2]$, as recorded in Antarctic ice, lag Antarctic

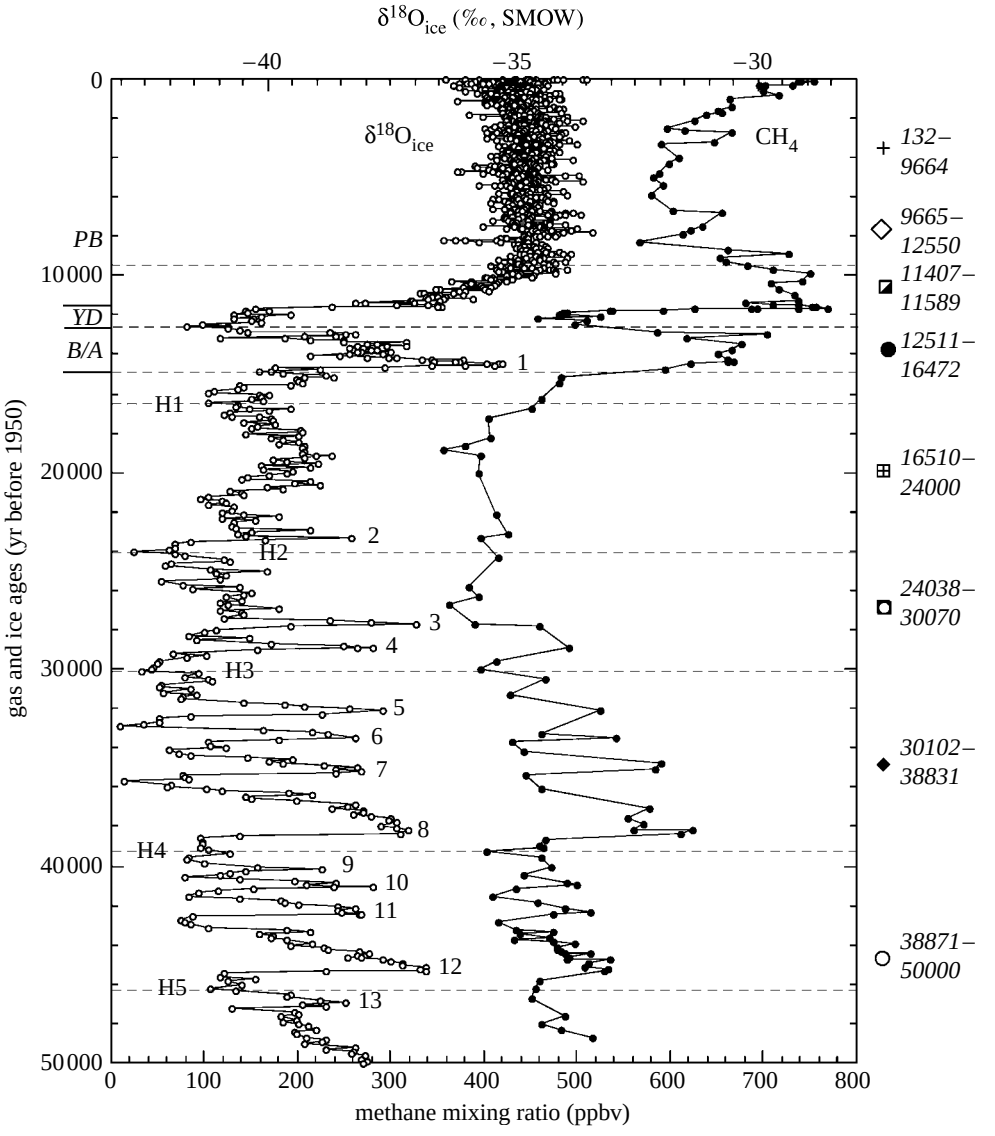

Figure 1. Time-series of Greenland GISP2 ice core record of $[CH_4]$ and $\delta^{18}O_{ice}$ for past 50 kyr (see text for references). The methane uses GISP2 gas ages and $\delta^{18}O_{ice}$ uses ice ages. H1–H5 indicate the Heinrich events, the numbers 1–13 identify the Dansgaard–Oeschger events. Numbers on the right of the plot are time intervals (separated by dashed lines) and their symbols are also used in figure 3.

temperature by *ca* 800 years e.g. Caillon *et al.* (2003). Similarly, for this period, Sowers & Bender (1995) reported that atmospheric $[CO_2]$ and $[CH_4]$ rose 2000–3000 years prior to the warming in the Northern Hemisphere.

Figure 1 is a traditional time-series representation of the $\delta^{18}O_{ice}$ and $[CH_4]$ for the past 50 kyr of the Greenland GISP2 ice core datasets. These GISP2 $\delta^{18}O_{ice}$ measurements are an indicator of local temperature and were reported by Grootes *et al.* (1993), Meese *et al.* (1994), Steig *et al.* (1994), Stuiver *et al.* (1995) and Grootes & Stuiver (1997). The GISP2 methane concentrations and gas ages

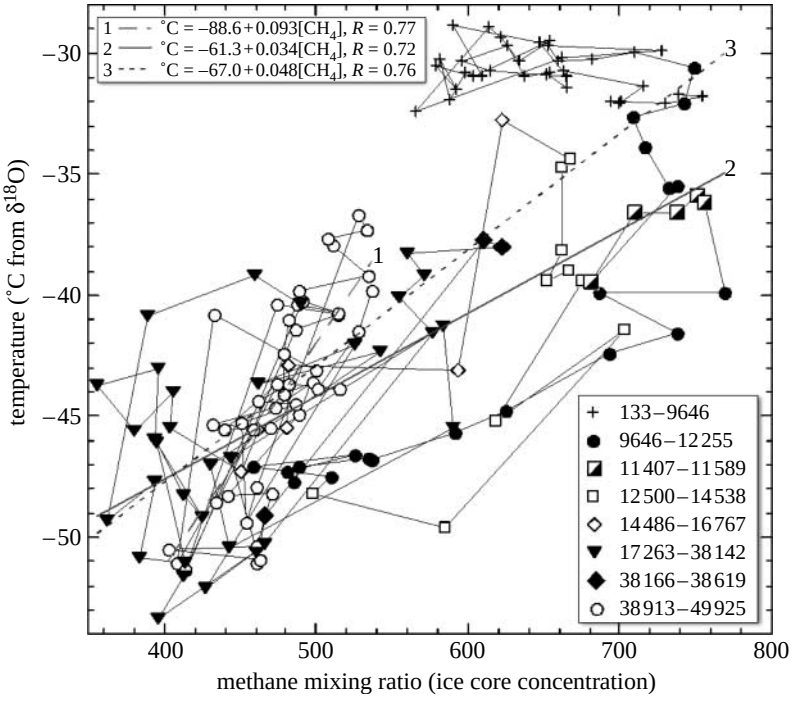

Figure 2. Relationships of $[CH_4]$ with temperatures recorded in the Greenland GISP2 ice core for the past 50 kyr BP (see text for references). Different correlations are observed for the various time periods indicated. The Holocene clearly departs from this temperature–$[CH_4]$ relationship.

are from Brook *et al.* (1996, 2000). Figure 1 also shows the Heinrich (H1-5) and Dansgaard–Oeschger (1–13) events observed in the GISP2 core. All data are hosted by ncdc.noaa.gov/pub/data/paleo/icecore/greenland/summit/gisp2. The relationships between $\delta^{18}O_{ice}$ and $[CH_4]$ are generally inferred only through visual inspection. This mode of comparison is largely necessary due to the uncertainty in aligning the gas age scales with the ice age.

To further elucidate these anticipated relationships, figure 2 plots the Greenland palaeotemperature against $[CH_4]$ for the youngest 50 kyr in the GISP2 core. The palaeotemperatures for GISP2 are calculated using transfer functions from corresponding GISP2 $\delta^{18}O_{ice}$ measurements as reported by Cuffey & Clow (1997) and Alley (2000, 2004). Figure 2 is constructed by harmonizing the ice and gas ages, i.e. by matching depths (nearest ice age temperature to $[CH_4]$ gas age). In addition to sampling and analytical uncertainties, the GISP2 data in figure 2 are subject to (i) factors other than temperature that affect $\delta^{18}O_{ice}$, (ii) errors in the calculation of temperature from $\delta^{18}O_{ice}$ measurements (oxygen isotope temperature sensitivity (α), i.e. $\Delta\delta^{18}O_{ice}/\Delta T$), and (iii) errors in the absolute and relative ice and gas ages.

The factors affecting $\delta^{18}O_{ice}$, such as seasonality and proximity of precipitation, sea-surface conditions and atmospheric circulation, have been discussed in detail by numerous authors, including Paterson (1994), Cuffey *et al.* (1995), Boyle (1997), Fawcett *et al.* (1997), Jouzel *et al.* (1997), Krinner *et al.* (1997), Werner *et al.* (2001) and Masson-Delmotte *et al.* (2005). The α value has been shown to

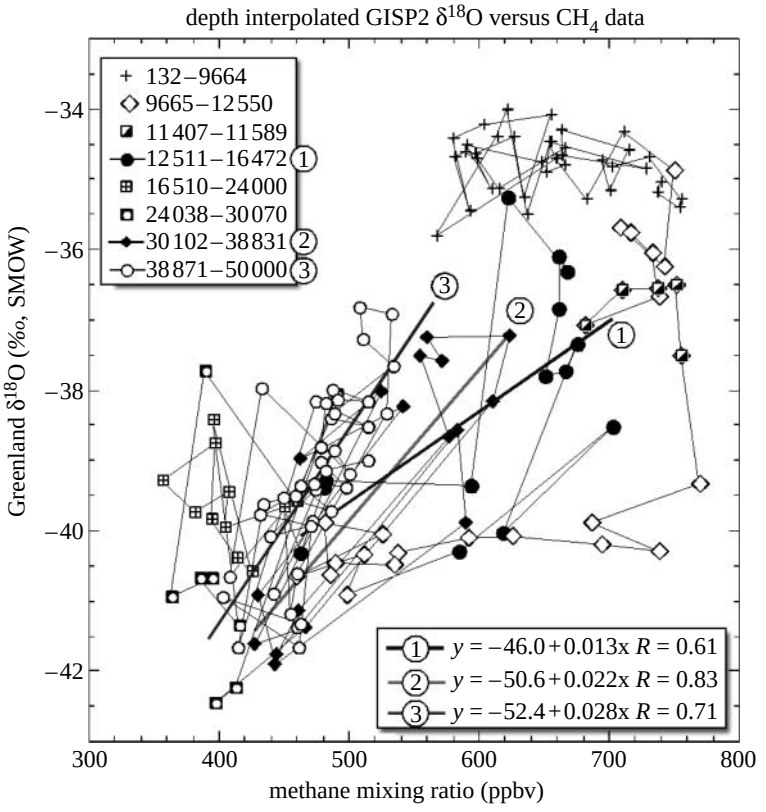

Figure 3. Relationships of $\delta^{18}O_{ice}$–$[CH_4]$ recorded in the Greenland GISP2 ice core for the past 50 kyr BP (see text for references). Different correlations are observed for the various time periods indicated (see figure 1). The plot uses GISP2 gas ages for $[CH_4]$ and interpolated GISP2 ice ages for $\delta^{18}O_{ice}$. SMOW, standard mean ocean water.

vary over time. The present day α value is estimated at 0.67‰ K^{-1} (Johnsen *et al.* 1989), while estimates of the Holocene α value range from 0.53 to 0.67‰ K^{-1} (Cuffey *et al.* 1994, 1995). An α value of 0.3‰ K^{-1} for the Younger Dryas (YD) was reported by Cuffey *et al.* (1995) and Johnsen *et al.* (1995) and this was later substantiated with gas isotope ages by Severinghaus *et al.* (1998), Grachev & Severinghaus (2005) and Huber *et al.* (2006). Using the work of Schwander *et al.* (1997), Lang *et al.* (1999) reported an α value of 0.4–0.5‰ K^{-1} for the Dansgaard–Oeschger events between 20 and 40 kyr BP. The accuracy of the α value for a chosen age translates directly into the accuracy of the temperature. To test this, figure 3 is a plot of GISP2 $\delta^{18}O_{ice}$ against $[CH_4]$, constructed by using interpolated $\delta^{18}O_{ice}$ ice ages to fit the $[CH_4]$. Figure 3 produces essentially the same plot as in figure 2. This points out that the changes observed in temperature and methane are much larger than any error associated with the chosen α value.

Uncertainty created by errors in the absolute ice ages (estimated as approx. 2% by Severinghaus & Brook (1999)) does not affect the temperature–methane relationships because the error is applicable to both the ice and the gas ages. Estimating the relative difference between the ice and gas ages is however a source of error of potentially $\leq$100 years. This is related to the confidence in

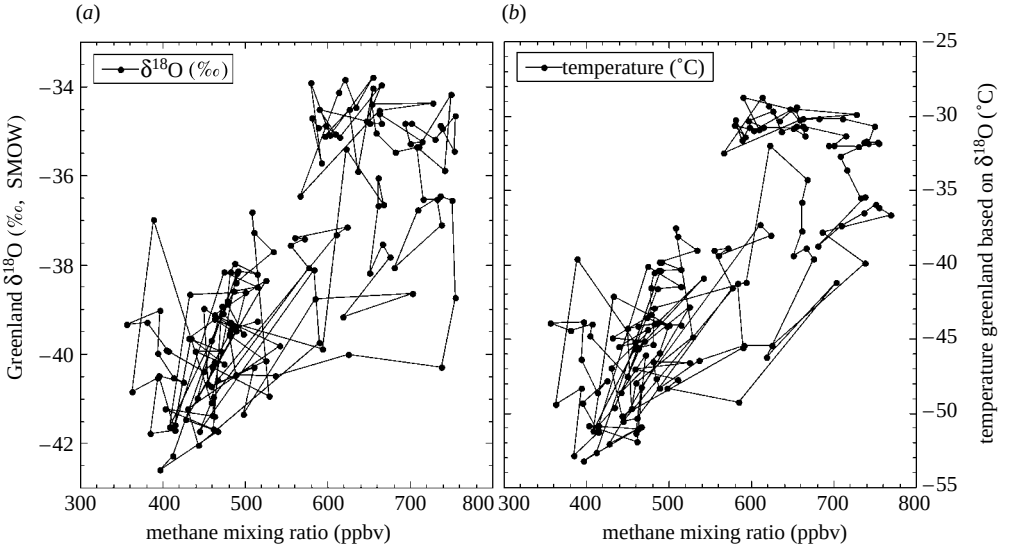

Figure 4. Sensitivity plots of (*a*) mismatched GISP2 $\delta^{18}O$ versus CH_4 data and (*b*) mismatched GISP2 temperature (from $\delta^{18}O$) versus CH_4 data recorded in the Greenland GISP2 ice core for the past 50 kyr BP. Gas and ice ages are purposefully shifted (mismatched) by up to 200 years to assess robustness of relationships seen in figures 2 and 3 to age matching uncertainties.

determining the closure age (Δage = gas age − ice age difference; Brook *et al.* 2000). It is also due to the fact that the ice taken for the gas measurements is not identical in age to ice samples taken for $\delta^{18}O_{ice}$. The uncertainty increases somewhat with depth, but with a few exceptions is $\leq$100 years. We tested the robustness of the temperature–methane and $\delta^{18}O_{ice}$–$[CH_4]$ relationships observed in figures 2 and 3 by purposefully misaligning (shifting) temperature and $\delta^{18}O_{ice}$ ice ages by up to 187 years too young and 168 years too old relative to the interpolated ice ages. Figure 4 shows that the patterns seen in figures 2 and 3 are largely maintained despite the age displacement, indicating that over century-range age intervals, the age matching is not critical.

Acknowledging age-scale uncertainties and sensitivities, we feel it is valuable to make the following observations. In general, figure 2 demonstrates the well-established trend towards increasing methane mixing ratios with increasing local temperatures. The linear regression through the entire dataset (line 3), although potentially a spurious correlation, reveals an approximately 20 ppbv increase in $[CH_4]$ with each 1°C rise. In addition, figure 2 indicates some other interesting features. We divided the 50 kyr BP dataset into several time blocks, reflecting various time periods of interest. For example, the Holocene data (133–9 646 years BP) are clearly segregated from the rest of the data. These warmer Holocene data (approx. −30°C) have no apparent relationship to temperature, despite an approximately 200 ppbv range in $[CH_4]$. Excluding the Holocene data, the $[CH_4]$–temperature correlation (line 2) drops to an approximate 1°C rise with a 30 ppbv increase in $[CH_4]$. In addition, the older data (38 913—49 925 years BP) indicate a tight, steeper trajectory (line 1) of approximately 1°C rise with a 10 ppbv increase in $[CH_4]$. Four examples of shorter transitions are given in figure 2 for (i)

11 407–11 589 years BP i.e. the YD–Preboreal period (YD–PB), discussed in more detail in this paper, (ii) 12 500–14 538 years BP, (iii) 14 486–16 767 years BP, and (iv) 38 166–38 619 years BP. These all occupy distinct regions of the $[CH_4]$–temperature diagram. Similarly, the $\delta^{18}O_{ice}$–$[CH_4]$ relationships show the age segmentation as shown in figure 3.

The correlation between $[CH_4]$ and $\delta^{18}O_{ice}$, and hence the derived Greenland temperatures, given by figure 3, indicate a teleconnection between the climate in Greenland and that of methane producing regions, including those controlled by tropical monsoon (Wang *et al.* 2001; Hughen *et al.* 2004). The important implication of figures 2 and 3 is that this teleconnection is not constant and is subject to subtle variations even over relatively short geological time spans. These are probably governed by different climate conditions within and since the last ice age. The point is that caution is required when reconstructing latitudinal climate connections from the Greenland $[CH_4]$–temperature relationship. However, the variations in the $[CH_4]$–temperature relationship may also provide clues for understanding the interdependence of North Atlantic and tropical climate.

The variations in $[CH_4]$ observed in figures 2 and 3 beg the question as to their cause. Are different intensities of the source fluxes (even those that are intermittent) and/or of the sinks changing the atmospheric methane burden on these time scales? Or, are the same sources and/or sinks changing their intensities with time? To address these questions, we use the combination of methane source and sink flux estimates together with their corresponding carbon and hydrogen stable isotope ratios ($\delta^{13}CH_4$ and $\delta D\text{-}CH_4$). This paper examines atmospheric methane budgets for four time periods, namely (i) Modern, (ii) PIH (approx. 300–2000 years BP), (iii) YD–PB transition (approx. 11.4–12.2 years BP), and (iv) Late Glacial Maximum (LGM; approx. 18 000 years BP). In particular, the objective is to combine the first reported $\delta^{13}CH_4$ and $\delta D\text{-}CH_4$ measurements in ice for palaeoatmospheres.

2. Source–sink components of Modern global methane inventory

Various approaches are used to estimate the Modern fluxes of methane to the atmosphere. These include inverse modelling, e.g. Hein *et al.* (1997), Houweling *et al.* (2000), Law & Vohralik (2001), Enting (2002), Butler *et al.* (2004), Michalak *et al.* (2005) and Chen & Prinn (2006), satellite measurements, e.g. SCIAMACHY (Frankenberg *et al.* 2005, 2006) and bottom-up mass balance approaches, e.g. Matthews & Fung (1987), Cicerone & Oremland (1988), Stevens & Engelkemeir (1988), Aselmann & Crutzen (1989), Houghton *et al.* (1990), Fung *et al.* (1991), Whiticar (1993), Lelieveld *et al.* (1998), Lassey *et al.* (2000) and Kaplan *et al.* (2006).

For the purposes of this paper, we do not rederive the Modern budgets, rather we use them to guide us in predicting past budgets. Considerable uncertainty exists in estimating the magnitude of the major source fluxes. To illustrate this, Keppler *et al.* (2006) recently reported aerobic methane production (AMP) from plants, a previously unknown source. Their scaled estimate for the global emission of methane from this source was 62–236 Tg yr^{-1}, i.e. potentially the largest single source of atmospheric methane. Subsequently, Houweling *et al.* (2006) reduced this to between 85 and 125 Tg yr^{-1}, i.e. similar to methane flux strength estimated for wetlands (approx. 140 Tg yr^{-1}; Kaplan 2002). To balance

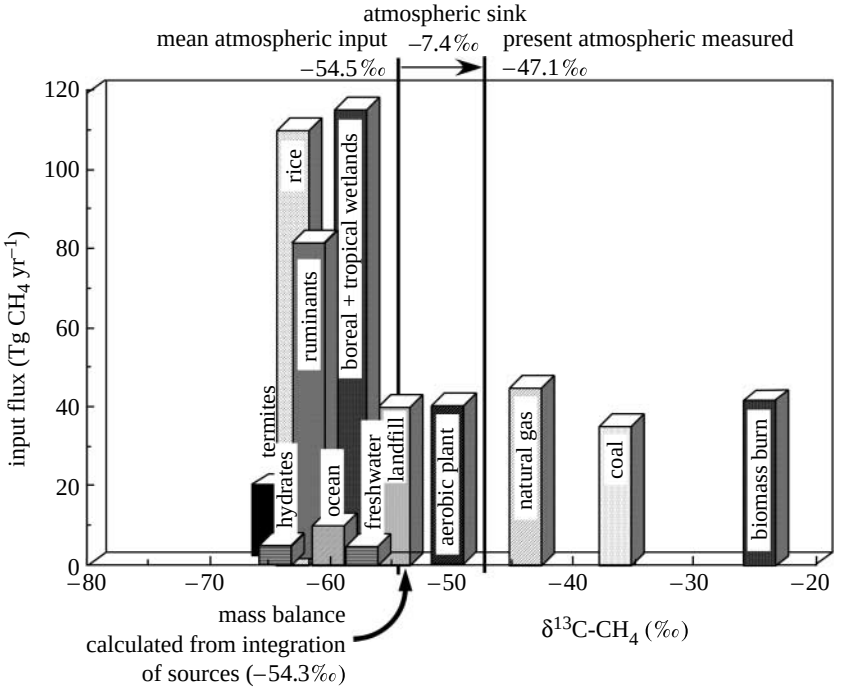

Figure 5. Histogram of modern global tropospheric flux magnitudes and $\delta^{13}CH_4$ of primary methane sources. The integrated input $\delta^{13}CH_4$ signal from the sources (δC_{in}) is indicated, as are the measured present $\delta^{13}CH_4$, the tropospheric CH_4 sink isotope fractionation ($\varepsilon_{C_{wt}}$) and the back-calculated mean atmospheric input $\delta^{13}CH_4$ (*measured mean input*).

the accomodate in the global methane source budgets while incorporating AMP, it is necessary to decrease other sources, particularly wetlands. Otherwise, these are most likely to be redundantly, i.e. double accounted, with AMP.

Difficulties in assigning accurate mean $\delta^{13}CH_4$ and $\delta D\text{-}CH_4$ values for the different sources also remain (note, all stable isotope ratios are reported as per mil relative to the Vienna Pee Dee Belemnite (VPDB) and Vienna standard mean ocean water (VSMOW) standards). For example, estimates of the mean $\delta^{13}CH_4$ for termite emissions vary between -41 and $-82‰$ (Tyler *et al.* 1988; Sugimoto *et al.* 1998; Tayasu 1998). The extreme variability largely reflects the taxonomy and diet of the termites (Boutton *et al.* 1983) and the degree of oxidation (Zimmerman *et al.* 1982). The challenges of using the correct mean $\delta D\text{-}CH_4$ values are exemplified by biomass burning. Early work by Whalen *et al.* (1990), Whalen (1993) and Whiticar (1993) suggested $\delta D\text{-}CH_4$ for biomass burning from -90 to $-300‰$. More recently, Snover *et al.* (2000) reported a mean value of $-210‰$, which contrasts with the estimated global $\delta D\text{-}CH_4$ value of $-169‰$ calculated by Yamada *et al.* (2006). We use a $\delta D\text{-}CH_4$ value of $-225‰$ for biomass burning in this paper.

Despite the problems in attributing fluxes or isotope signatures to the major sources, we can use the Modern values to provide us with a framework/baseline for the expected relative changes in the three past ages that we examine here. In addition, we can incorporate the sink terms for the different ages to estimate the tropospheric budget. Figures 5 and 6 show, for present day, the flux strengths of the

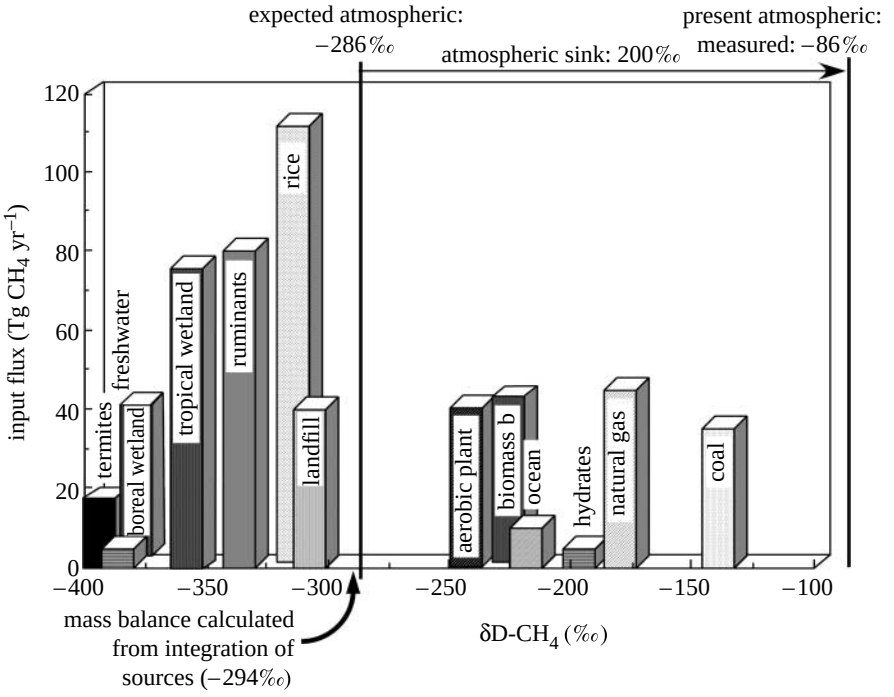

Figure 6. Histogram of modern global tropospheric flux magnitudes and δD-CH_4 of primary methane sources. The integrated input δD-CH_4 signal from the sources (δD_{in}) is indicated, as are the measured present δD-CH_4, the tropospheric CH_4 sink isotope fractionation ($\varepsilon_{D_{wt}}$) and the back-calculated mean atmospheric input δD-CH_4 (*measured mean input*).

primary sources of tropospheric methane and their respective carbon and hydrogen isotope ratios. Rice paddies are the single largest source at 110 Tg yr^{-1}, but the combination of tropical and boreal wetland fluxes exceed this with 115 Tg yr^{-1} (table 1). Although uncertain, we assign a value of only 40 Tg yr^{-1} for AMP, and have decremented the wetland contribution accordingly. We do not assign a flux for the Modern geological source (natural seepages of thermogenic methane; table 1), but we have accommodated this and the corresponding anthropogenic emissions under natural gas and coal emissions (45 and 35 Tg yr^{-1}, respectively).

The $\delta^{13}CH_4$ values for the various sources range from approximately −25 to −65‰. The range in δD-CH_4 is −140‰ (coal) to −390‰ (termites). Using the values in table 1, the carbon and hydrogen isotope ratio mass balance ($F_{iT}\delta_{iT}$) for the source inputs can be calculated by the simple linear mixing equation,

$$F_{iT}\delta_{iT} = \{F_{i1} + \delta_{i1} + \cdots + F_{in}\delta_{in}\}_{sources}, \tag{2.1}$$

where F_{ix} are the source fluxes (Tg yr^{-1}), and the isotope ratio of the individual sources is δ_{ix}. A carbon isotope mass balance from the sources is calculated by equation (2.1) to have a weighted mean $\delta^{13}CH_4$ of −54.2‰ (termed δC_{in} in table 1) as shown in figure 2. The corresponding mean δD-CH_4 of the sources (δD_{in}) is −294‰ (table 1; figure 6).

Four primary sinks of atmospheric methane are considered, i.e. (i) tropospheric abstraction with hydroxyl radicals (OH•), e.g. Saueressig *et al.* (2001), (ii) soil uptake, e.g. Ridgwell *et al.* (1999), (iii) stratospheric removal, e.g. Rice *et al.* (2003),

Table 1. Fluxes and stable carbon and hydrogen isotope ratios of major methane sources and sinks for four time periods. The δC_{in} and δD_{in} are the mass balances for carbon and hydrogen based on equation (2.1). The $\varepsilon_{C_{wt}}$ and $\varepsilon_{D_{wt}}$ are the total sink carbon and hydrogen isotope offsets. The *calculated atmospheric* isotope values are $\delta C_{in}+\varepsilon_{C_{wt}}$ and $\delta D_{in}+\varepsilon_{D_{wt}}$. The *measured atmospheric* is the measured or anticipated value, and the *expected mean input* is the measured atmospheric minus ε_{WT}.

	age											
	Modern			Preindustrial Holocene			Younger Dryas			Late Glacial Maximum		
source	flux ($Tg\ yr^{-1}$)	$\delta^{13}CH_4$ (‰)	δD-CH_4 (‰)	flux ($Tg\ yr^{-1}$)	$\delta^{13}CH_4$ (‰)	δD-CH_4 (‰)	flux ($Tg\ yr^{-1}$)	$\delta^{13}CH_4$ (‰)	δD-CH_4 (‰)	flux ($Tg\ yr^{-1}$)	$\delta^{13}CH_4$ (‰)	δD-CH_4 (‰)
rice paddies	110.0	−63.0	−320	0.0	0.0	0.0						
ruminants	80.0	−60.5	−330	12.0	−56.8	−330	13.5	−57.8	−330	15.0	−57.6	−330
natural gas	45.0	−44.0	−180	0.0	−41.8	−180	0.0	−41.8	−180	0.0	−41.8	−180
coal	35.0	−37.0	−140	0.0			0.0			0.0		
biomass burning	41.0	−24.6	−225	3.9	−25.6	−225	3.7	−26.2	−225	3.4	−25.7	−225
boreal wetlands	38.0	−62.0	−380	21.0	−62.0	−380	12.0	−62.0	−380	3.0	−63.0	−380
tropical wetlands	77.0	−58.9	−360	35.0	−56.8	−380	30.0	−57.4	−380	20.0	−58.0	−380
termites	16.0	−63.0	−390	16.0	−62.2	−390	15.5	−62.2	−390	13.0	−62.7	−390
landfills	40.0	−55.0	−310	0.0			0.0			0.0		
ocean	10.0	−58.0	−220	10.0	−58.0	−220	7.0	−58.0	−220	7.0	−58.0	−220
freshwater	4.0	−53.8	−385	3.9	−53.8	−385	4.0	−53.8	−385	4.0	−53.8	−385
gas hydrates	4.0	−62.5	−190	3.9	−62.5	−190	1.6	−62.5	−190	0.0	−62.5	−190
geological	0.0	−41.8	−200	35.0	−41.8	−200	35.0	−41.8	−200	35.0	−41.8	−200
AMP	40.0	−51.2	−260	50.0	−49.4	−260	42.0	−49.8	−260	30.0	−49.9	−260
δX_{in} (δC_{in}, δD_{in})		−54.2	−295		−52.6	−298		−52.2	−296		−51.3	−287
expected mean input		−54.5	−286					−52.4	−295		−48.7	−287
$\varepsilon_{X_{wt}}(\varepsilon_{C_{wt}}, \varepsilon_{D_{wt}})$		7.4	200		7.0	200		6.4	200		5.7	200
calculated atmospheric	540	−46.8	−95	191	−45.6	−98	164	−45.8	−96	130	−45.6	−87
measured atmospheric	540	−47.1	−86	190	?	?	157	−46.0	−95	130	−43.0	−87

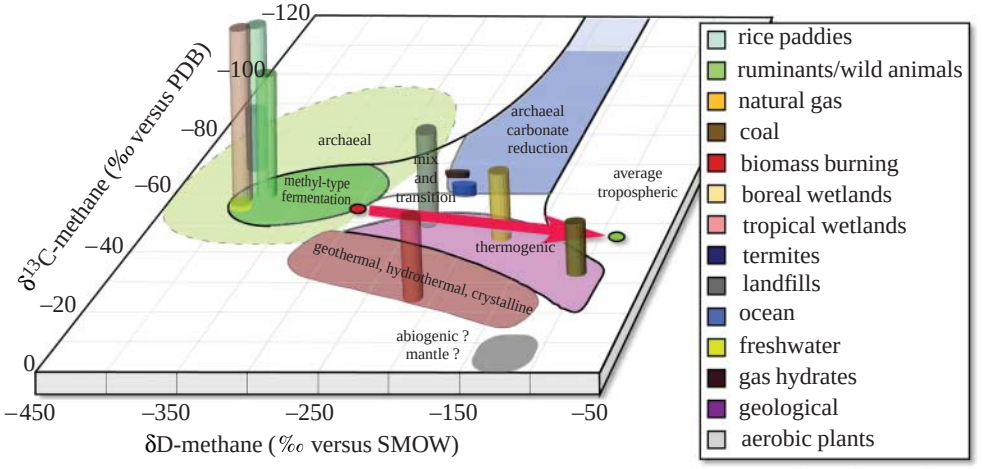

Figure 7. Combination $\delta^{13}CH_4$ and $\delta D\text{-}CH_4$ plot showing the major methane types (based on Whiticar 1999). The primary, Modern tropospheric methane sources and their respective flux strengths are shown. The integrated input $\delta^{13}CH_4$–$\delta D\text{-}CH_4$ signal from the sources (δC_{in} and δD_{in}) and the sink fractionation ($\varepsilon_{C_{wt}}$ and $\varepsilon_{D_{wt}}$) are also indicated.

and (iv) reaction of CH_4 and $Cl\cdot$ in the marine boundary layer (MBL), e.g. Allan *et al.* (2005). Each sink is associated with an isotope effect that leads to isotopic fractionation (α_{o_x}). The combined sink isotope fractionation can be recast in equation (2.2) as the isotope offset ($\varepsilon_{X_{wt}}$), i.e.

$$\varepsilon_{X_{wt}} \approx 10^3 \ln\{F_{o_1}\alpha_{o_1} + \cdots + F_{o_n}\alpha_{o_n}\}_{sinks} \approx 10^3\left(1 - \{F_{o_1}\alpha_{o_1} + \cdots + F_{o_n}\alpha_{o_n}\}_{sinks}\right), \tag{2.2}$$

where F_{o_x} are the sink fluxes (Tg yr^{-1}). The first three sinks combine to give an effective weighted total carbon isotope offset $\varepsilon_{C_{wt}}$ of 7.4‰, which is used in this paper. We currently do not account for the MBL sink, but considering the work of Allan *et al.* (2005), future budgets may need to do so. The associated hydrogen isotope offset caused by the tropospheric methane sink ($\varepsilon_{D_{wt}}$) is 200‰.

The *calculated atmospheric* isotope value (δ_T) is calculated using both the source and the sink terms in the net carbon and hydrogen isotope ratio mass balance ($F_T\delta_T$) according to equation (2.3)

$$\delta_T = [\{F_{i1}\delta_{i1} + \cdots + F_{in}\delta_{in}\}_{sources}]/F_T - \varepsilon_{X_{wt}}. \tag{2.3}$$

Using the bottom-up estimates of δ_{in}, the mean source input ($\delta^{13}CH_4$, −54.2‰; $\delta D\text{-}CH_4$, −295‰), and the sink isotope shifts ($\varepsilon_{C_{wt}}, \varepsilon_{D_{wt}}$), the calculated atmospheric $\delta^{13}CH_4$ is −46.8‰ and the net $\delta D\text{-}CH_4$ is −95‰ (table 1; figures 5 and 6). The calculated atmospheric values can be compared with the current, global *measured atmospheric* measured values for $\delta^{13}CH_4$ of −47.1‰ (Miller *et al.* 2002) and $\delta D\text{-}CH_4$ of −86‰ (Whalen 1993; Quay *et al.* 1999; Bergamaschi *et al.* 2000). The difference between the measured atmospheric and calculated atmospheric estimates is relatively small for $\delta^{13}CH_4$ (0.3‰), but larger (9‰) for $\delta D\text{-}CH_4$. This illustrates the ongoing challenge in assigning the correct fluxes and/or isotope ratios. If we anchor the mass balance with the current measured

atmospheric $\delta^{13}CH_4$ and $\delta D\text{-}CH_4$ values of -47.1 and $-86‰$ and incorporate the sink isotope shifts ($\varepsilon_{C_{wt}}, \varepsilon_{D_{wt}}$), we can back-calculate the isotope ratio of the global expected mean input of methane to the troposphere. In this case, the expected mean input $\delta^{13}CH_4$ is $-54.5‰$ and $\delta D\text{-}CH_4$ is $-286‰$ (table 1), compared with δC_{in} of $-54.2‰$ and δD_{in} of $-295‰$. The discrepancies point to the deficiencies we have in describing the source and sink fluxes. Presently, we do not have an *a priori* way to improve the budgets, and the discrepancies remain.

It is interesting to note in figure 5 that many of the sources have carbon isotope ratios approximately $-60‰$, i.e. close to δC_{in}. This is expected and indicative of the dominant Archaeal origin for the majority of the methane. Most of the leverage towards a ^{13}C-richer input to δC_{in} is provided by biomass burning, landfills, coalbed methane and natural gas emissions (Whiticar 1994). All of these are largely anthropogenic-influenced sources. AMP is presently somewhat of a wildcard, as both the source magnitudes and the isotope ratios (especially $\delta D\text{-}CH_4$) need to be better defined.

A different distribution is seen for $\delta D\text{-}CH_4$ in figure 6. The $\delta D\text{-}CH_4$ signatures of the sources congregate into two primary groups i.e. one group with $\delta D\text{-}CH_4$ less than $-300‰$ and a second with $\delta D\text{-}CH_4$ greater than $-250‰$. This segregation largely reflects the δD_{water} associated with the source and the methane formation pathway involved (Whiticar 1999).

The combination of tropospheric $\delta^{13}CH_4$ and $\delta D\text{-}CH_4$ together with the total net flux i.e. sources − sinks, do not provide sufficient constraints to unambiguously model the tropospheric methane budget (e.g. Whiticar 1993; Lassey *et al.* 2000; Bréas *et al.* 2001). However, the isotope signatures of the different sources do occupy specific regions of a $\delta^{13}CH_4$ versus $\delta D\text{-}CH_4$ plot, i.e. CD diagram (Whiticar *et al.* 1986). Figure 7 is the CD diagram for present day methane depicting the fields of the various methane origins, such as thermogenic, geothermal and methanogenic. The latter, i.e. Archaeal methane, is traditionally labelled with the misnomer 'bacterial' or 'biogenic' methane. The column heights of the methane sources shown in figure 7 are proportional to their flux strengths. Also shown in figure 7 is the integrated mean $\delta^{13}CH_4$ and $\delta D\text{-}CH_4$ input values (δC_{in}, δD_{in}) and the current calculated atmospheric $\delta^{13}CH_4$ and $\delta D\text{-}CH_4$. The list of methane sources shown along the side of figure 7 include some that are not important in Modern tropospheric methane budgets, but factor into the palaeoatmospheres, as discussed below. Although various sources are scattered across the plot, there is an aggregation of several larger sources in the sector of figure 7 that is associated with methyl-type fermentation by Archaeans.

3. Source components of PIH, YD–PB and LGM global methane inventories

Recognizing the uncertainty in the Modern inventory, estimates in palaeobudgets of tropospheric methane can be made in a relative sense. Essentially, we attempt to determine how the global palaeoenvironment has changed and how these changes translate into shifts in the methane source and sink fluxes and isotope signatures. The influence of these factors on the $\delta^{13}CH_4$ of source types for the PIH, YD–PB and LGM is treated in detail by Schaefer & Whiticar (in press). For these timeframes, methane concentration studies have been made on numerous ice cores from Greenland and the Antarctic, including the Vostok and GISP2 cores

(e.g. Craig & Chou 1982; Chappellaz *et al.* 1993*a*, 1997; Brook *et al.* 1996, 2000; Etheridge *et al.* 1998, Petit *et al.* 1999; Dällenbach *et al.* 2000; Stauffer *et al.* 2002). In contrast, only a few isotope measurements have been made on non-Modern methane. These currently include $\delta^{13}CH_4$ determinations by Craig *et al.* (1988), Ferretti *et al.* (2005), Sowers *et al.* (2005), Schaefer *et al.* (2006), Sowers (2006*a*) and Schaefer & Whiticar (2007). The only values for palaeo-δD-CH_4 from ice-core samples are published by Sowers (2006*b*). As a consequence, the available constraints on the palaeoatmospheric budgets are currently limited to these few $\delta^{13}CH_4$ and δD-CH_4 measurements.

Certainly changes to the inventory of sources, such as the addition of anthropogenic sources, can differentiate Modern budgets from those in the past. However, there are several ways in which changes in the environment can over time alter not only the fluxes, but also the isotope signatures of sources and sinks of methane. These, in turn, shift the global $\delta^{13}CH_4$ and δD-CH_4 budget. A primary factor is changes to the isotope signature of organic matter that serves as methane precursors. This includes (i) substrates for methanogenesis e.g. wetlands, termites, etc., (ii) kerogen for natural gas (coal, thermogenic or geothermal gas), or (iii) fuel for biomass burning. Environmentally related changes to the sinks can also exert control on the methane isotope budgets.

Changes to the carbon isotope ratio of organic matter ($\delta^{13}C_{org}$), which serves as precursor substrates for methanogenesis, can potentially lead to systematic shifts in $\delta^{13}CH_4$. These organic compounds are predominantly produced and obtain their signature through plant biosynthesis. The $\delta^{13}C$ of plant matter depends directly on atmospheric $\delta^{13}CO_2$, (e.g. White *et al.* 1994; Gröcke 2002), as well as on the photosynthetic pathways (Calvin–Benson cycle and Hatch–Slack cycle, i.e. C_3 and C_4 photosynthesis, respectively) and various environmental parameters, such as water tensions, temperature and biostressors (e.g. infestations).

Schaefer & Whiticar (in press) studied how fluctuations in atmospheric $\delta^{13}CO_2$ for PIH and LGM as recorded in ice cores and plant fossils changed the $\delta^{13}CH_4$ of various methane sources. The same work also examines the influence of shifts in C_3 and C_4 vegetation, as modelled by Collatz *et al.* (1998), on the carbon isotope signature of various source types. The latter are sensitive to these climatically induced vegetation changes, because C_3 and C_4 plants carry different isotope signatures of approximately -27 and -15‰, respectively, e.g. Ehleringer *et al.* (1997), which are passed on to the methane generated from these precursor materials. Detailed calculations of potential changes in source $\delta^{13}CH_4$ are presented in Schaefer & Whiticar (in press), and the following is a short summary of the relevant information.

Plant fossils indicate a 1.1‰ ^{13}C-enrichment of atmospheric $\delta^{13}CO_2$ during the PIH, relative to the present (Marino *et al.* 1992), in good agreement with $\delta^{13}CO_2$ reconstructions from ice cores by Francey *et al.* (1999) and Smith *et al.* (1999). Marino *et al.* (1992) also reported a relative 0.4‰ ^{13}C-enrichment in $\delta^{13}CO_2$ during glacial conditions. Ice-core data reveal a ^{13}C-enrichment of $\delta^{13}CO_2$ by 0.9‰ in the LGM and a 0.4‰ ^{13}C- enrichment versus today during the YD cold period. Thus, all things equal, the shift in $\delta^{13}C_{org}$ transfers into a similar shift in the $\delta^{13}CH_4$ of methanogenic emissions.

$\delta^{13}CH_4$ changes caused by C_3–C_4 vegetation shifts are difficult to assess, e.g. relative expansion of grasslands (Prentice *et al.* 1993; Steudler *et al.* 1996). However, if the amount generated remains constant for each type, then a shift in

the proportion of C_3 and C_4 can transfer into a similar shift in the $\delta^{13}CH_4$ of the emissions. Collatz *et al.* (1998) reported that C_4-dominated grasslands increased from 70% at the LGM to 74% in the PIH, then dropped to the present day 57% due to anthropogenic land conversion and rising [CO_2]. This is reflected in our methane budgets. Although the C_3/C_4 is poorly constrained, vegetation models by Kaplan *et al.* (2004) supported the findings of Collatz *et al.* (1998). Furthermore, Schaefer (2005) found that even a $\pm 50\%$ change in C_3–C_4 methane fluxes resulted in an atmospheric $\delta^{13}CH_4$ shift of only 0.6‰.

Ruminants will produce methane with a $\delta^{13}CH_4$ dependent on the ratio of C_3 and C_4 in their diet i.e. a 12‰ difference in $\delta^{13}CH_4$ for C_3 versus C_4, as shown by Rust (1981), Metges *et al.* (1990), Ehleringer & Monson (1993), Levin *et al.* (1993), Schulze *et al.* (1998) and Bilek *et al.* (2001). The proportion of C_3 versus C_4 plants will also impact the $\delta^{13}CH_4$ emitted from wildfires. For example, Chanton *et al.* (2000) reported for biomass burning $\delta^{13}CH_4$ ranges of -26 to -30‰ for C_3 forest fires versus -17 to -26‰ for C_4 grass fires. Today's average biomass burning $\delta^{13}CH_4$ is calculated to be -24.6‰ according to data from Hao & Ward (1993). The C_3 versus C_4 change with time translates to a wildfire average $\delta^{13}CH_4$ of -26.6‰ in the PIH and -26.7‰ in the LGM (Schaefer & Whiticar in press).

AMP has also been shown to depend on whether the plant type is C_3 or C_4. Keppler *et al.* (2006) report a shift of approximately 6‰ in AMP $\delta^{13}CH_4$ derived from C_3 versus C_4. This can result in AMP $\delta^{13}CH_4$ of -50.5‰ for the PIH and -49.9‰ for the LGM.

Strangely, Tyler *et al.* (1988) found no diet relationships between C_3 and C_4 plants for the $\delta^{13}CH_4$ produced by termites in various habitats, even within a single species. As this is unlike all the other methanogenic sources, Schaefer & Whiticar (in press) incorporated a C_3–C_4 response. They calculated a termite-derived $\delta^{13}CH_4$ of -62.2‰ for the PIH and -62.7‰ for the LGM, compared to a Modern value of -63.0‰.

It is complicated to quantify production of methane from various wetlands and to assign representative isotope signatures. Methanogenesis and the derived $\delta^{13}CH_4$ in wetland systems respond to the influences of

(i) climate and temperature, i.e. magnitude changes of isotope effects (Blair *et al.* 1993; Botz *et al.* 1996; Whiticar 1999; Walter & Heimann 2000; Fey *et al.* 2004),
(ii) dominance of the methanogenic pathway, i.e. methyl fermentation (MF) or carbonate reduction (CR; Whiticar *et al.* 1986),
(iii) the fraction of precursor material utilized,
(iv) isotope fractionation during diffusion, advection and transport (e.g. Alperin *et al.* 1988; Chanton 2005), and
(v) microbial oxidation (e.g. Whiticar & Faber 1986; Tyler *et al.* 1994).

These factors suggest that there should be a significant difference in $\delta^{13}CH_4$ between glacial and interglacial wetlands. Determining a representative value for the boreal wetlands remains difficult, even for Modern conditions. For example, Bellisario *et al.* (1999) reported $\delta^{13}CH_4$ values between -50‰ and -73‰ for minerotrophic systems, whereas Chanton *et al.* (2000) and Bowes & Hornibrook (2006) found $\delta^{13}CH_4$ values ranging from -70 to -90‰. Such ^{13}C-depleted values

are very difficult to reconcile for the PIH, YD or LGM budgets (table 1). Realizing the uncertainty, we use more traditional $\delta^{13}CH_4$ values of −62‰ for the Modern, PIH and YD boreal wetlands. To give an indication of the sensitivity of the chosen $\delta^{13}CH_4$ for boreal wetlands, values of −70 and −80‰ for the Modern budget would shift the δC_{in} to −47.3 and −48.0‰, respectively. The former is comparable to the measured tropospheric $\delta^{13}CH_4$ value of −47.1‰, but the latter would require adjustments to other sources to comply. The PIH and YD budgets can accommodate a boreal wetland $\delta^{13}CH_4$ of −70‰ (δC_{in} shifts to −53.5 and −52.8‰, respectively), but the LGM remains poorly unbalanced. Boreal wetland $\delta^{13}CH_4$ values of −80‰ for the PIH, YD and LGM do not reconcile well. Schaefer & Whiticar (in press) estimate that LGM wetland $\delta^{13}CH_4$ was more ^{13}C-depleted than in the PIH by 0.3–0.9‰, depending on the MF-derived fraction (f_{MF}) relative to CR production. The temperature-dependent carbon isotope fractionation contributes to this ^{13}C-depletion of $\delta^{13}CH_4$ in the LGM with 0.3–0.4‰. A shift from MF to CR at lower temperatures could have led to an additional contribution of 0.3–0.5‰. As a result, a $\delta^{13}CH_4$ value of −63‰ is used for the boreal wetlands in the LGM budget. Similarly, $\delta^{13}CH_4$ of tropical wetlands varied by up to 2.1‰ between the LGM and Modern (table 1). Based on this, Schaefer & Whiticar (in press) suggested that glacial–interglacial temperature changes have an impact on the CH_4 isotope mass balance that is detectable in ice-core measurements (table 1).

The above mentioned factors influencing the carbon isotope ratio of the tropospheric methane sources are summarized in table 2. The magnitudes of the relative changes in $\delta^{13}CH_4$ for the different sources between the LGM and PIH, and between the PIH and Modern are illustrated in figure 8. Note that sink components are not incorporated into this figure. Clearly the shifts in $\delta^{13}CH_4$ are generally greater between the PIH and today, than between the LGM and PIH. In addition, the PIH–Modern comparisons frequently show ^{12}C-enrichments for the present sources with $\delta^{13}CH_4$ shifts of 1–4‰, due to human intervention. In contrast, the LGM–PIH show more limited differences, with modest ^{12}C-enrichment during the glacial period. The flux weighted mean (δC_{in} in figure 8) reflects this with the δC_{in} approximately +2‰ for PIH-Modern, yet δC_{in} approximately +0.6‰ for the LGM–PIH.

As mentioned, palaeo-$\delta D\text{-}CH_4$ are currently more speculative and less well constrained. On the other hand, several of the environmental factors that can shift $\delta^{13}CH_4$ are not applicable to the $\delta D\text{-}CH_4$ systematics. To a large extent, $\delta D\text{-}CH_4$ is controlled by δD_{water}. For example, Whiticar *et al.* (1986), Burke *et al.* (1988), Sugimoto & Wada (1995), Hornibrook *et al.* (1997), Waldron *et al.* (1999) and Whiticar (1999) and others showed that in methanogenesis the $\delta D\text{-}CH_4$ is dependent on the MR or CR pathway, i.e. if the hydrogen is transferred from organic substrates or H_2. Ultimately, the $\delta D\text{-}CH_4$ for either pathway is determined by δD_{water}. Similarly, the $\delta D\text{-}CH_4$ in non-methanogenic sources such as coal, natural gas and probably AMP, have their $\delta D\text{-}CH_4$ set by δD_{org}, which is also determined by δD_{water}. The challenge is to determine the appropriate hydrogen isotope effects for the different methane forming processes, and then applying the correct adjustments, i.e. temperature dependence, change in ocean and meteoric δD_{water}. For the purposes of this paper, the $\delta D\text{-}CH_4$ for each source and time period uses the present day value. For AMP, a $\delta D\text{-}CH_4$ value of −260‰ is currently assigned (Frank Keppler 2006, personal communication). Table 1 lists the representative $\delta D\text{-}CH_4$ values taken from a merger of different estimates for Modern methane sources (e.g. Whiticar 1990, 1993;

Table 2. Effects of changes in environmental conditions on global tropospheric $\delta^{13}CH_4$ of sources and sinks for the Late Glacial Maximum (LGM), Preindustrial Holocene (PIH) and Modern ages.

	LGM	PIH	Modern
1A changes in atmospheric $\delta^{13}CO_2$ and hence methane precursor material			
^{13}C-enrichment in $\delta^{13}CO_2$ in PIH, 0.4‰ in glacial			
e.g. Marino *et al.* (1992), Francey *et al.* (1999) and Smith *et al.* (1999)			
^{13}C-enrichment in $\delta^{13}CO_2$	0.4‰	1.1‰	0
1B changes in C_3 versus C_4 vegetation			
C_3 $\delta^{13}C_{org}$ approximately −27‰ versus C_4 $\delta^{13}C_{org}$ approximately −15‰			
e.g. Prentice *et al.* (1993), Ehleringer *et al.* (1997) and Collatz *et al.* (1998)			
C_4 grasslands	70%	74%	57%
(a) changes in C_3 versus C_4 vegetation: effect on ruminants			
C_3 cows: $\delta^{13}CH_4$ approximately −69‰ C_4 cows: $\delta^{13}CH_4$ approximately −54‰⇒$\Delta\delta^{13}$CH of 15‰			
e.g. Rust (1981), Stevens & Engelkemeir (1988), Metges *et al.* (1990), Ehleringer & Monson (1993), Levin *et al.* (1993), Schulze *et al.* (1998) and Bilek *et al.* (2001)			
$\delta^{13}CH_4$ wild animals	−58.5‰	−57.9‰	−60.5‰
(b) changes in C_3 versus C_4 vegetation: effect on wild fires (biomass burning)			
C_3 fires: $\delta^{13}CH_4$ approximately −17–26‰ C_4 fires: $\delta^{13}CH_4$ approximately −26 to 30‰			
e.g. Wright & Bailey (1982), Hao & Ward (1993), deBano *et al.* (1998) and Chanton *et al.* (2000)			
average $\delta^{13}CH_4$ fires	−26.7‰	−26.6	−24.6‰
(c) changes in C_3 versus C_4 vegetation: effect on termite emissions			
no observed correlation of termite emitted $\delta^{13}CH_4$ to C_3 versus C_4 diet!			
e.g. diet: Tyler *et al.* (1988), termites: Zimmerman *et al.* (1982); palaeoveg.: Prentice *et al.* (1993)			
average $\delta^{13}CH_4$ termites	−62.7‰	−62.7‰	−63.9‰
(d) changes in C_3 versus C_4 vegetation: effect on aerobic methane production (AMP)			
$\Delta\delta^{13}CH_4$ C_3 AMP versus C_4 AMP: approximately 6‰			
e.g. AMP: Houweling *et al.* (2006) and Keppler *et al.* (2006); NPP: François *et al.* (1998)			
average AMP $\delta^{13}CH_4$	−49.9‰	−49.4‰	−51.2‰
2A temperature dependence of methanogenesis			
KIEs (expressed by α) are temperature-dependent			
carbonate reduction: $\ln \alpha_{CR} = (23/T) - 0.022$			
e.g. Blair *et al.* (1993), Whiticar (1993), Botz *et al.* (1996) and Fey *et al.* (2004)			
average α_{CR}	1.062 (8°C)	1.061 (12°C)	1.060 (15°C)
2B temperature dependence of methane consumption			
KIEs (expressed by α) are temperature-dependent, but may not control			
do not know yet, probably small			
3A sinks net to gross CH_4 emission (N/G)			
Modern wetlands N/G approximately 0.6 (40% CH_4 oxidized during transport)			
Q_{10} values of oxidation approximately 50% less T sensitive than methanogenesis			
e.g. Bellisario *et al.* (1999), Walter & Heimann (2000) and Chanton (2005)			
N/G	*ca* 0.53		*ca* 0.60
3B tropospheric hydroxyl			
KIE (α_{OH}) = 1.0039–1.0054. Loss rate depends on T and [CH_4] but not α_{OH}			
e.g. Cantrell *et al.* (1990), Fung *et al.* (1991), Staffelbach *et al.* (1991), Martinerie *et al.* (1995), Tans (1997), Saueressig *et al.* (2001), Valdes *et al.* (2005) and Kaplan *et al.* (2006)			
OH· abundance	higher?	higher?	
3C soil methane consumption			
KIEs (expressed by α_{soil}) are temperature-dependent, and diffusion is important as are land use, soil moisture, ecosystem			
e.g. King *et al.* (1989), Tyler *et al.* (1994), Martinerie *et al.* (1995), Steudler *et al.* (1996), Reeburgh *et al.* (1997), Ridgwell *et al.* (1999), Brook *et al.* (2000), Snover & Quay (2000) and Kaplan (2002)			
estimates of α_{soil}	1.0272 7°C cooler		1.017–1.022
rates (Tg yr^{-1})	*ca* 0.6 (starved)	*ca* 14	*ca* 37

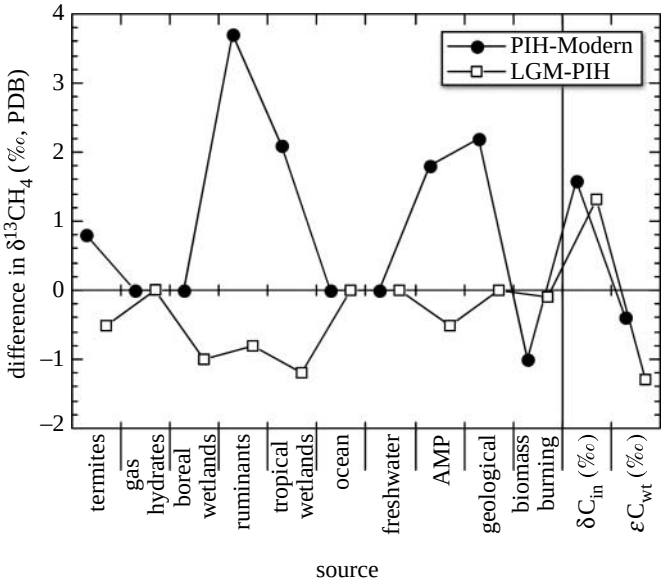

Figure 8. Relative changes in $\delta^{13}CH_4$ for the primary tropospheric methane sources between (*a*) Modern (solid circles) and Preindustrial Holocene (PIH) and (*b*) Late Glacial Maximum (LGM) and PIH (open squares), based on changes to environmental drivers. The sources are ordered on *x*-axis according to Modern $\delta^{13}CH_4$ values. The integrated input $\delta^{13}CH_4$ signal from the sources (δC_{in}) and sinks ($\varepsilon_{C_{wt}}$) are also shown. Note that the Modern geological source includes natural and anthropogenic gas emissions, which have slightly different $\delta^{13}CH_4$ values (table 1).

Snover *et al.* 2000). These source δD-CH_4 values are combined with their $\delta^{13}CH_4$ and scaled by their flux magnitude in figure 7. The resultant flux weighted mean tropospheric input δD-CH_4 (δD_{in}) is calculated using equation (2.1) and also shown in figure 7. To estimate δD_{in} for the three older time periods, the individual methane source fluxes for the PIH, YD–PB and LGM as derived from Chappellaz *et al.* (1993*b*) are used to scale the relative proportions of each methane source. The resulting δD_{in} are listed in table 1.

To compare the shifts in the source $\delta^{13}CH_4$, δD-CH_4 and flux magnitudes for the Modern, PIH, YD–PB and LGM ages, a series of CD diagrams with flux histograms are plotted in figure 9. Although there are substantial changes in the fluxes, the changes in $\delta^{13}CH_4$ and δD-CH_4 are subtle. The flux weighted mean tropospheric inputs (δC_{in} and (δD_{in}) are shown in figure 9, but their subtle differences with ages are more clearly illustrated by the expanded *mean of source inputs* box in figure 10.

4. Sink components of the PIH, YD–PB and LGM global methane inventories

The sinks of atmospheric methane are mercifully less diverse than the sources. As mentioned above, the four primary are

(i) abstraction with hydroxyl radicals (OH•) in the troposphere (Cantrell *et al.* 1990; Staffelbach *et al.* 1991; Martinerie *et al.* 1995; Saueressig *et al.* 2001),
(ii) soil uptake (King *et al.* 1989; Ridgwell *et al.* 1999),

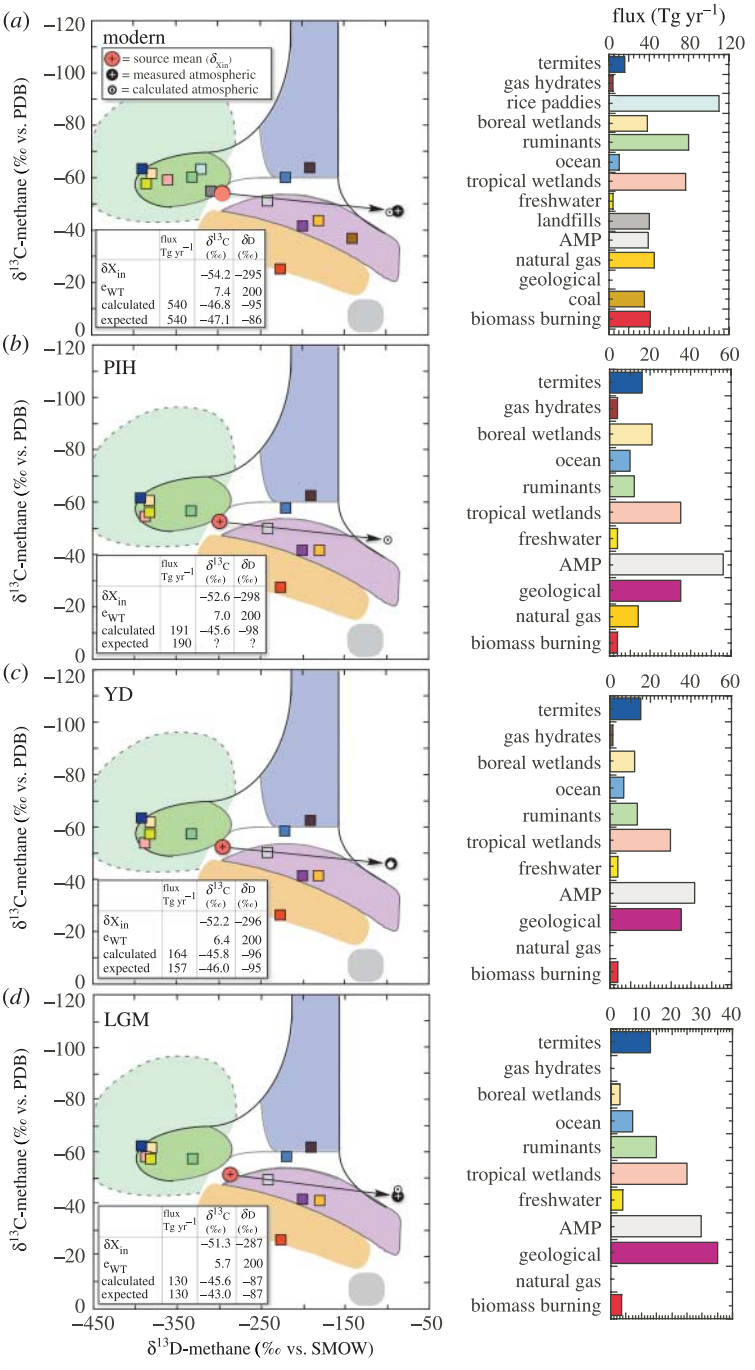

Figure 9. $\delta^{13}CH_4$ and δD-CH_4 plots for the (*a*) Modern, (*b*) Preindustrial Holocene (PIH), (*c*) Younger Dryas (YD), and (*d*) Late Glacial Maximum (LGM) showing the changes in the isotope signals from the primary tropospheric methane sources. The integrated input $\delta^{13}CH_4$–δD-CH_4 signals from the sources (δC_{in} and δD_{in}) and the sink fractionations ($\varepsilon_{C_{wt}}$ and $\varepsilon_{D_{wt}}$) are indicated. The types and flux magnitudes of the major methane sources are also shown as histograms. The *calculated* $\delta^{13}CH_4$ and δD-CH_4 values in the embedded table are δ_{in}–$\varepsilon_{X_{wt}}$). The *measured* $\delta^{13}CH_4$ and δD-CH_4 values are based on measurements in air or ice.

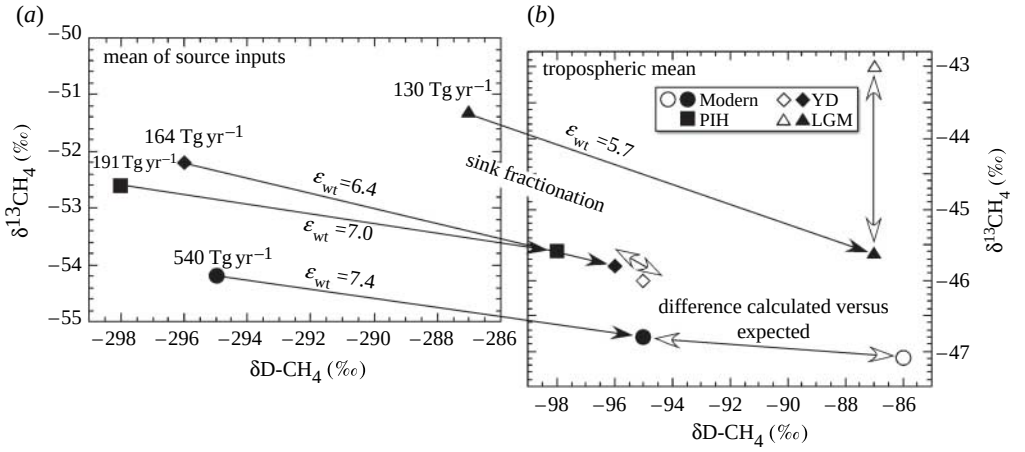

Figure 10. Expanded $\delta^{13}CH_4$ and δD-CH_4 plots for the Modern, Preindustrial Holocene (PIH), Younger Dryas (YD) and Late Glacial Maximum (LGM) showing the isotope trajectories of tropospheric methane for (*a*) integrated input $\delta^{13}CH_4$–δD-CH_4 signal from the sources (δC_{in} and δD_{in}) and (*b*) the *calculated* values ($\delta_{in} - \varepsilon_{Xwt}$) (closed symbols). The *measured* $\delta^{13}CH_4$ and δD-CH_4 values (open symbols) are based on measurements in air or ice. The total methane fluxes and sink fractionations ($\varepsilon_{C_{wt}}$ and $\varepsilon_{D_{wt}}$) for the four ages are also given.

(iii) stratospheric removal (McCarthy *et al.* 2001; Rice *et al.* 2003), and
(iv) chlorine sink, particularly in the MBL (Wang *et al.* 2002; Allan *et al.* 2005).

The magnitude of the isotope effects for each sink carries some uncertainty, but typically the reaction rate constants are faster for $^{12}CH_4$ than the common isotopologues $^{13}CH_4$ or $^{12}CH_3D$ e.g. Gordon & Mulac (1975), Davidson *et al.* (1986, 1987), Alperin *et al.* (1988), Cantrell *et al.* (1990), Tyler *et al.* (1994, 2000), Saueressig *et al.* (1995, 2001), Reeburgh *et al.* (1997), Snover & Quay (2000), and Michelsen & Simpson (2001). The result of these sinks is an enrichment of the residual tropospheric methane in ^{13}C and ^{2}H relative to the mean of the source inputs. The magnitudes of the sinks are discussed in detail in Schaefer & Whiticar (in press) and earlier by Staffelbach *et al.* (1991), and are summarized in table 2. The isotope shifts due to the Modern combined sinks are $\varepsilon_{C_{wt}}$ of 7.4‰ for carbon and $\varepsilon_{D_{wt}}$ of 200‰ for hydrogen. However, different environmental conditions in the PIH, YD–PB and LGM compared with today, lead to different values for $\varepsilon_{X_{wt}}$. We estimate $\varepsilon_{C_{wt}}$ for the PIH as 7.0‰, YD–PB as 6.4‰ and LGM as 5.7‰ (table 1). Although $\varepsilon_{D_{wt}}$ cannot yet be accurately defined for the palaeo-ages, Sowers (2006*b*) suggested that it could have changed in the range of +3.4‰ and −1.6‰ between the PIH and LGM. For this paper, we use the Modern $\varepsilon_{D_{wt}}$ of 200‰ for all four ages. We recognize and accept the limitation this places on our calculations.

The effect that these calculated changes in $\varepsilon_{C_{wt}}$ and processes that affect the $\delta^{13}CH_4$ of source types have on atmospheric $\delta^{13}CH_4$ in the past is shown in figure 11. It is important to note that here these budget reconstructions are not intended or adjusted to match past atmospheric $\delta^{13}CH_4$ values that have been measured in ice. The latter would require us to rebalance the source inventories, which we attempt later in the paper. Rather, the values summarized in table 2 and shown in figure 11 illustrate the fact that past environmental changes affected

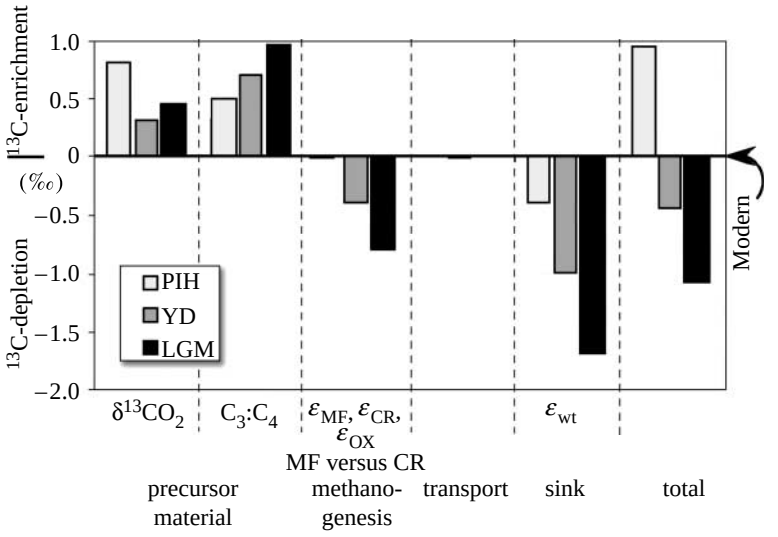

Figure 11. Summary of relative $^{13}CH_4$ enrichments/depletions of environmental and process drivers on $\delta^{13}CH_4$ for the Preindustrial Holocene (PIH), Younger Dryas (YD) and Late Glacial Maximum (LGM) relative to Modern (zero-line; modified from Schaefer & Whiticar in press).

atmospheric $\delta^{13}CH_4$ through changes in $\delta^{13}CH_4$ of the sources and in sink isotope fractionation. It should be emphasized that the $\delta^{13}CH_4$ could be affected even if the source inventory, i.e. the relative magnitude of individual fluxes, had remained the same. However, we recognize that some sources do, in fact, undergo higher changes in their isotopic signature than others. To address the issue that the studied changes affect $\delta^{13}CH_4$ in addition to, but not independently of, the source inventory, we based the reconstructions shown in figure 11 on source fluxes derived from Chappellaz *et al.* (1993*b*). We then calculated the difference in the isotope mass balance between a scenario with modern source $\delta^{13}CH_4$ values and sink fractionation and a scenario where the environmental changes in the latter are included. To illustrate this, figure 11 shows the relative importance of the changes in source and sink on $\delta^{13}CH_4$ for the PIH, YD–PB and LGM relative to Modern (0‰ line). An interesting detail is our finding that the environmental changes should lead to a small (approx. 1‰) ^{13}C-depletion in the LGM, while first results (Sowers 2006*a*; Vas Petrenko 2006, unpublished data) show that atmospheric $\delta^{13}CH_4$ is strongly enriched in ^{13}C. Obviously, a higher percentage of ^{13}C-rich emissions overwhelms the changes in $\delta^{13}CH_4$ of individual sources and sinks.

5. Constraining the PIH, YD–PB and LGM with $\delta^{13}CH_4$ and δD-CH_4

Bottom-up source scenarios for the past, based on vegetation models and geological evidence, can be constrained by the isotope mass balances, because a valid scenario must produce a calculated atmospheric isotope signature that matches the ice core results. Despite the fact that for every time period a

multitude of scenarios is possible, the isotopic constraints improve the budget reconstructions by discriminating against models that violate the mass balance or exceed the uncertainty of the parameters. Using the parameters derived above, we adjusted the source fluxes of bottom-up source scenarios in order to best match the isotopic mass balance for both $\delta^{13}CH_4$ and $\delta D\text{-}CH_4$. The resulting methane budgets for PIH, YD–PB and LGM (table 1) are not unique solutions to the problem, but represent our best guess.

Plugging the δC_{in} and $\varepsilon_{C_{wt}}$ values in table 1 into equation (2.3) results in calculated atmospheric $\delta^{13}CH_4$ values of -45.6, -45.8 and -45.6‰ for the PIH, YD–PB and LGM, respectively. These are all ^{13}C-enriched compared with the present day calculated atmospheric $\delta^{13}CH_4$ of -46.8‰, by 1–2‰.

Similarly, using δD_{in} and $\varepsilon_{D_{wt}}$ equation (2.3) gives calculated atmospheric $\delta D\text{-}CH_4$ values of -98, -96 and -87‰ for the PIH, YD–PB and LGM. Methane for the palaeo-periods is enriched in ^{2}H relative to today (calculated atmospheric $\delta D\text{-}CH_4 = -95$‰) by up to 9‰. These age differences in both calculated atmospheric $\delta^{13}CH_4$ and $\delta D\text{-}CH_4$ are demonstrated in figure 10 for the Modern, PIH, YD–PB and LGM.

The differences between each age represent the composite of the chosen source isotope ratios, the fractionation of the sinks and the magnitude of the source fluxes. In the case of the Modern, the accuracy of δ_{in} and $\varepsilon_{X_{wt}}$ can be evaluated by comparison with direct measurement of tropospheric air samples. To evaluate the PIH, YD–PB and LGM, we resort to ice samples to find the measured atmospheric isotopic signature for each age (Ferretti *et al.* 2005; Schaefer *et al.* 2006; Sowers 2006*a*,*b*; Schaefer & Whiticar in press).

6. Reconciliation of LGM budgets

The methane budget for the LGM, as presented in table 1 and figures 9 and 10, was developed using the reconstructions for past source $\delta^{13}CH_4$ and sink fractionation from Schaefer & Whiticar (in press) and flux estimates as derived from palaeovegetation models and geological evidence. The resulting calculated atmospheric $\delta D\text{-}CH_4$ of -87‰ agrees well with measured atmospheric $\delta D\text{-}CH_4$ of -87‰ by Sowers (2006*b*). In contrast, our $\delta^{13}CH_4$ budget predicts a calculated atmospheric value of approximately -45.6‰, whereas the first results of measured atmospheric values for the LGM (Sowers 2006*a*; Vas Petrenko 2006, unpublished data) indicate that the real values may be up to 3–4‰ more ^{13}C-rich than our budget reconstruction in table 1 suggests, i.e. $\delta^{13}CH_4$ of -43‰. The reconstructions of source type $\delta^{13}CH_4$ and sink fractionation by Schaefer & Whiticar (in press) are already incorporated in the YD and LGM budgets. The overall impact (figure 11) is a small ^{13}C-depletion in glacial and near-glacial conditions and cannot account for or contribute to the observed ^{13}C-enrichment.

In order to resolve the discrepancy between calculated atmospheric and measured atmospheric values, we attempt here to reconcile the budget having a source inventory with the appropriate isotope mass balance. Only two, or possibly three, natural sources (biomass burning, geological and perhaps AMP) are sufficiently ^{13}C-enriched to account for the offset, i.e. to drive the measured atmospheric to -43‰. It should be noted that for every scenario of adjusting the

sources for new values of δC_{in} and δD_{in}, it was still not possible to fully reconcile all constraints, namely: (i) measured atmospheric $\delta^{13}CH_4$ and $\delta D\text{-}CH_4$, (ii) flux, and (iii) YD budget.

Firstly, biomass burning from wildfires is the most ^{13}C-enriched source. However, its natural emissions account for less than 3% of the total source. In order to balance the budget to the preliminary LGM $\delta^{13}CH_4$ data, wildfire emissions would have to be seven times higher (greater than 10% of the total). Although this would hardly break the constraints set by $\delta D\text{-}CH_4$, geological evidence does not support such high emissions from biomass burning at late glacial times (Haberle & Ledru 2001).

Secondly, to satisfy the budget, the geological emissions could be increased threefold over the values listed in table 1, to the point that they would account for 50% of the total source. Luyendyk *et al.* (2005) suggested that at lower glacial sea level, more gas seeps were exposed and raised geological emissions to up to twice the Modern amount. Two arguments stand against such high geological emissions. For one, they would lead to $\delta D\text{-}CH_4$ values that are 25‰ more depleted in ^{2}H than measured. For another, estimated total flux for the LGM would double, which has to be reconciled with sink rates and known atmospheric $[CH_4]$. An additional consideration is that sea-level controlled geological emissions would also be part of the YD budget. At this time, sea-level rise had reached about 50% of the glacial transition (Fairbanks 1989), suggesting that about half the additional geological flux at the LGM must be included in the YD budget. In fact, each process that could account for ^{13}C-enrichment at the LGM would also have to be accounted for in the YD budget and probably offset its mass balance.

Thirdly, AMP is a recently added source to methane budgets. As such, the range of carbon and hydrogen isotope values and how they could change over time is unknown. Although the $\delta^{13}CH_4$ has been measured for some Modern plants, the $\delta D\text{-}CH_4$ has not. A simple change of the AMP $\delta^{13}CH_4$ approximately from -49.9 to -40‰ could satisfactorily rebalance the budget, but it is unclear at this point why the AMP $\delta^{13}CH_4$ would change.

The requirement to adjust both the YD and the LGM methane budgets rules out several other possible explanations for the LGM ^{13}C-enrichment. Schaefer *et al.* (2006) list five processes that would lead to ^{13}C-enrichment of natural CH_4 budgets. These are higher than expected biomass burning, geological emissions, AMP, revised $\delta^{13}CH_4$ of tropical wetlands and the MBL sink. We are not aware of processes that would lead to substantial differences for AMP and the MBL sink between LGM and YD, beyond those that have been discussed by Schaefer & Whiticar (in press) and are incorporated in table 1. In contrast, a revised $\delta^{13}CH_4$ of tropical wetlands, in agreement with field measurements by Quay *et al.* (1991) and others, would affect the LGM budget far more than the YD budget. Dällenbach *et al.* (2000) used changes in the interpolar gradient in atmospheric $[CH_4]$ to show that tropical sources, i.e. foremost wetlands, made up 75% of the LGM budget, but only 55% during the YD.

We therefore present alternative methane budgets for the YD and the LGM in table 3. These mass balances include more ^{13}C-rich $\delta^{13}CH_4$ for tropical wetlands and an increase in geological methane emissions that is twice as high for the LGM as for the YD. In addition, the relative contributions of tropical and boreal wetlands for each time period were scaled to reflect the findings of

Table 3. Reconciliation of LGM budget by adjusting source δC_{in} and δD_{in}, with the constraints: (i) measured atmospheric $\delta^{13}CH_4$ and δD-CH_4, (ii) flux and (iii) YD budget.

	YD			LGM		
source	flux ($Tg\ yr^{-1}$)	$\delta^{13}CH_4$ (‰)	δD-CH_4 (‰)	flux ($Tg\ yr^{-1}$)	$\delta^{13}CH_4$ (‰)	δD-CH_4 (‰)
ruminants	11.5	−58.2	−330.0	12.7	−58.5	−330
biomass burning	3.1	−26.6	−225.0	2.9	−26.6	−225
boreal wetlands	18.0	−61.5	−380.0	3.5	−61.3	−380
tropical wetlands	26.7	−51.0	−380.0	19.0	−51	−380
termites	13.2	−62.4	−390.0	11.0	−62.7	−390
ocean	6.0	−58.2	−220.0	5.9	−58.2	−220
freshwater	3.4	−53.8	−385.0	3.4	−53.8	−385
gas hydrates	1.4	−62.5	−190.0	0.0	−62.5	−190
geological	42.0	−43.0	−200.0	55.0	−43.0	−200
AMP	28.5	−50.2	−260.0	16.0	−49.9	−260
$\delta X_{in}(\delta C_{in}, \delta D_{in})$		−51.4	−295		−49.3	−274
expected mean input		−52.4	−295		−48.7	−287
$\varepsilon_{X_{wt}}(\varepsilon_{C_{wt}}, \varepsilon_{D_{wt}})$		6.4	200		5.7	200
calculated atmospheric	154	−45.0	−95	130	−43.3	−74
measured atmospheric	157	−46	−95	130	−43.0	−87

Dällenbach *et al.* (2000). In combination, these changes lower the LGM $\delta^{13}CH_4$ strongly while affecting the YD value to a lesser degree. In order to counteract the effect that these changes have on the δD-CH4 mass balance, we also lowered the relative contribution of AMP in favour of the wetland source, while staying within the uncertainty ranges that follow from the work by Keppler *et al.* (2006) and Houweling *et al.* (2006).

The resulting mass balances are somewhat too enriched in ^{13}C for the YD and ^{2}H for the LGM, and too depleted in ^{13}C for the LGM, slightly exceeding the analytical uncertainties (± 0.3‰ for $\delta^{13}CH_4$). The persistent difficulties in reconstructing mass balance scenarios that satisfy the isotope constraints without contradicting geological evidence or modern observations of methane dynamics indicate substantial gaps in our knowledge of the methane system. It is probable that the LGM ^{13}C-enrichment cannot be explained with an appropriate mix of source fluxes alone, but may lie with an environmental control that has been either underestimated or not included in the reconstructions of Schaefer & Whiticar (in press). It is remarkable that the isotope records of Ferretti *et al.* (2005) show a strong shift in methane isotopes that is not associated with changing $[CH_4]$, while the records of Schaefer *et al.* (2006) and upon closer inspection also those of Sowers (2006*b*) show unperturbed isotope values during dramatic $[CH_4]$ changes. These findings suggest that mass balances that are solely driven by source inventories are not adequate to describe natural methane isotope dynamics. More insight may be gained from extended palaeorecords that may show correlations of $\delta^{13}CH_4$ and/or δD-CH_4 with other environmental parameters, such as global ice cover or atmospheric carbon dioxide concentration. Such findings may provide a more complete explanation for the glacial ^{13}C-enrichment.

7. Comparison of $\delta^{13}CH_4$ and $\delta D\text{-}CH_4$ for YD–PB

As mentioned, only a few measurements of palaeoatmospheric $\delta^{13}CH_4$ and $\delta D\text{-}CH_4$ have been made using firn air and ice samples. The best comparison currently available is for the YD–PB transition, a period with a rapid rise in $[CH_4]$ from approximately 450 ppbv to over 850 ppbv. This is possible by combining the Greenland GISP2 ice core $\delta D\text{-}CH_4$ data of Sowers (2006*b*) with the Greenland Pakitsoq ice sheet $\delta^{13}CH_4$ data of Schaefer *et al.* (2006).

Figure 12 shows the times series for the GISP2 and Pakitsoq ice sheets across the YD–PB transition from *ca* 12.4 to 11.2 kyr BP. Pakitsoq $\delta^{18}O_{ice}$, $[CH_4]$ and $\delta^{13}CH_4$ are in figure 12*a–c*, respectively, and figure 12*d* is the GISP2 $\delta D\text{-}CH_4$ data. The age scales for all plotted parameters have been adjusted to match the gas age scale of Severinghaus *et al.* (1998). The latter authors used tree-ring studies (Friedrich *et al.* 1999) to set the onset of the transition at 11 570 years BP ($\pm$10 years). The transition using the GISP2 time scale is *ca* 11 650 years BP. The difference emphasizes the ongoing challenge for a consistent, reliable chronology. Each data point represents approximately a 30-year interval. The greyed region in figure 12 covers the YD–PB transition (11.57–11.46 kyr BP) defined by Grachev & Severinghaus (2005), Petrenko *et al.* (2006) and Schaefer *et al.* (2006) based on the Pakitsoq $\delta^{15}N$, $\delta^{18}O_{ice}$, and $[CH_4]$.

The $\delta^{13}CH_4$ time series reveals two main features: (i) a ^{13}C-enrichment relative to today of approximately 1‰ (-46 versus -47‰ Modern) and (ii) no obvious carbon isotope change across the YD–PB transition. The shift between Modern and YD–PB is explained by Schaefer *et al.* (2006) and Schaefer & Whiticar (in press) to be due to environmental changes that shifted both source/sink signals and strengths. The second feature means that the rise in $[CH_4]$ is either just a proportional increase in the same sources during the entire interval, or that changes in the sources and/or sinks were somehow well balanced. Similarly, the $\delta D\text{-}CH_4$ data in figure 12 remain approximately constant around -95‰ up to *ca* 11.5 kyr BP. This is approximately 9‰ depleted in ^2H relative to the present day. At 11.49 and 11.08 kyr BP, $\delta D\text{-}CH_4$ drops to approximately -108‰, then -116‰, even more ^2H depleted than today. Sowers (2006*b*) attributes the differences in the YD–PB values from other ages due to a combination of factors, similar to those we postulate for carbon (§3), i.e. C_3–C_4 changes, temperature dependence of the OH-abstraction KIE and, additionally, changes in $\delta D\text{-}CH_4$ due to changes in δD_{water}.

The cross plot of $\delta^{13}CH_4$ and $\delta D\text{-}CH_4$ (figure 13) for the Schaefer *et al.* (2006) and Sowers (2006*b*) Greenland ice data for the YD reveal a most interesting feature for methane. An increase in ^{13}C-enrichment in the methane corresponds to an increase in ^2H-enrichment. There are also chronological sequences embedded in this $\delta^{13}CH_4$–$\delta D\text{-}CH_4$ relationship. From 12.15 to 11.83 kyr BP (segment 3 in figure 12, squares in figure 13) methane becomes enriched in ^2H and ^{13}C isotopes. This is during relatively isothermal conditions (figure 12*a*), and with no significant changes in $[CH_4]$. From 11.80 to 11.55 kyr BP (segment 2 in figure 12; circles in figure 13), the direction reverses (depletion in ^2H and ^{13}C isotopes), essentially on the same $\delta^{13}CH_4$–$\delta D\text{-}CH_4$ trajectory as segment 1. According to the findings of Severinghaus *et al.* (1998), this decades long time period when $[CH_4]$ was stable before the end-of-YD rise corresponds to a time of rapid temperature increase.

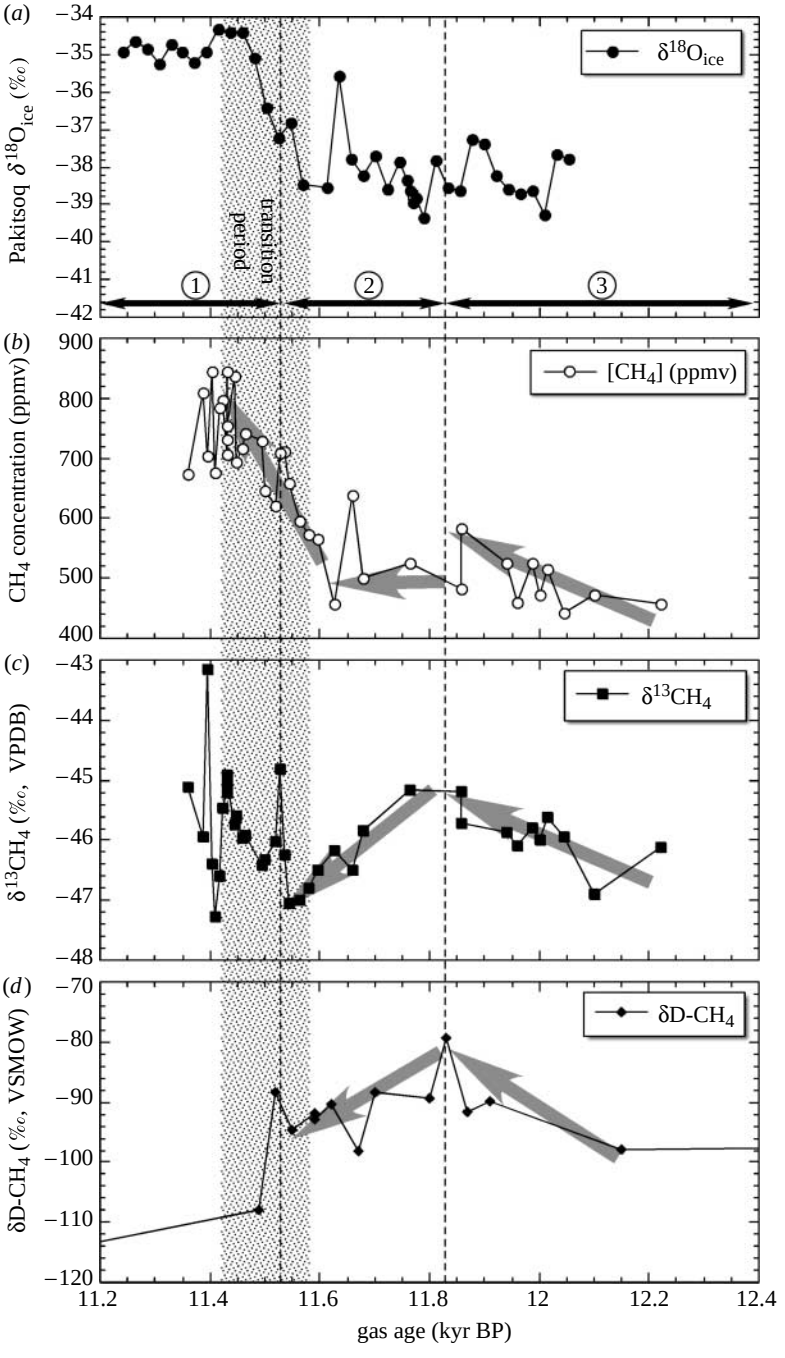

Figure 12. Comparison age plots across the YD–PB transition (12.4 to 11.2 kyr BP) for Greenland Pakitsoq ice sheet of (*a*) $\delta^{18}O_{ice}$ (Petrenko *et al.* 2006), (*b*) [CH_4] (Schaefer *et al.* 2006), (*c*) $\delta^{13}CH_4$ (Schaefer *et al.* 2006), and (*d*) GISP2 δD-CH_4 (Sowers 2006*b*). The stippled region is the YD–PB transition as determined by Pakitsoq data. The dashed lines demarcate the three time segments (circled numbers, figure 13). The greyed arrows indicate general trends discussed in the text. VPDB, Vienna Pee Dee Belemnite; VSMOW, Vienna standard mean ocean water.

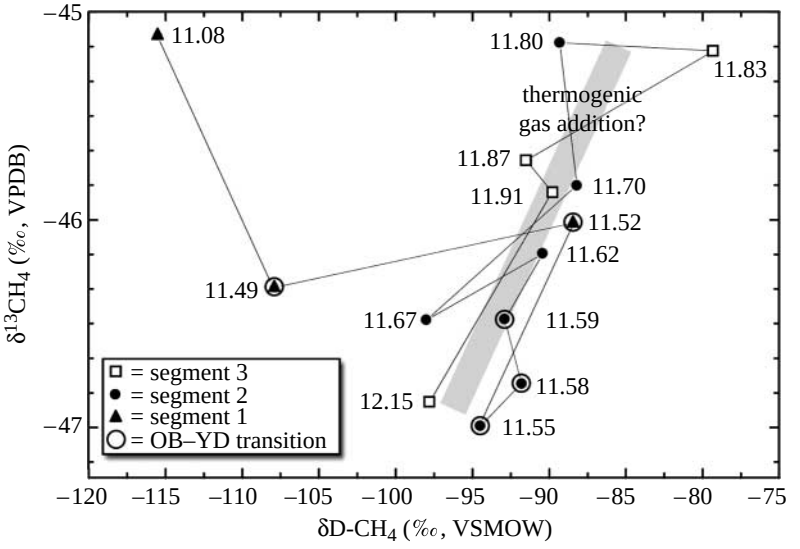

Figure 13. Expanded $\delta^{13}CH_4$ and δD-CH_4 plots of the Pakitsoq $\delta^{13}CH_4$ (Schaefer *et al.* 2006) and GISP2 δD-CH_4 (Sowers 2006*b*). The three segments shown in figure 12 and discussed in text are plotted as different symbols. The greyed line indicates the possible mixing trend and the circled symbols span the ages of the Younger Dryas–Preboreal (YD–PB) transition. VPDB, Vienna Pee Dee Belemnite; VSMOW, Vienna standard mean ocean water.

At 11.52 kyr BP, the trend reverses back to ^{2}H and ^{13}C enrichment, after the GISP2 temperature maximum has been reached and is starting to cool. By the end of the sequence at 11.49 and 11.08 kyr BP i.e. earliest PB, (segment 1 in figure 12, diamonds in figure 13) the $\delta^{13}CH_4$–δD-CH_4 relationship observed in the YD breaks down. These two PB data points have δD-CH_4 values approximately 15–30‰ lighter than those in the YD trend.

Although speculative, a possible explanation for the $\delta^{13}CH_4$–δD-CH_4 relationship of segments 1 and 2 is that the magnitude of ^{2}H and ^{13}C-rich methane source fluxes, such as coal-derived or thermogenic methane, or biomass burning are changing with time. For example, using the simple linear mixing equation (equation (2.1)) and varying only the geological flux in table 1 between 20 and 45 $Tg\,yr^{-1}$ for the different segments, the calculated atmospheric $\delta^{13}CH_4$–δD-CH_4 values shift from −46.8‰, −100‰ to −45.2‰, −85‰, respectively. For a more rigorous treatment, the total source fluxes need to be adjusted, but the example points out how fluctuating thermogenic gas fluxes alone could account for the $\delta^{13}CH_4$–δD-CH_4 relationship. If the decrease in the thermogenic source is related to the synchronous rapid rise in temperature, in this example it is unclear and we do not know of any mechanism to explain a causal relationship.

In the YD–PB transition period (segment 1, greyed in figure 12), the correspondence to thermogenic gas is not observed. In particular the δD-CH_4 values are substantially more ^{2}H-depleted than in the other segments, in fact more than in the entire Sowers (2006*b*) database. The youngest $\delta^{13}CH_4$ data from Schaefer *et al.* (2006) at 11.36 kyr BP was used to pair with the 11.08 kyr BP

data point of Sowers (2006*b*) in figure 13. Even if this $\delta^{13}CH_4$ value were incorrect, then it would not alter the fact that the PB δD-CH_4 values of segment 1 are substantially more depleted in ^{2}H than in the YD.

The $\delta^{13}CH_4$–δD-CH_4 signatures in segments 1 to 3 show that a massive Archaeal hydrate release, i.e. 'Clathrate Gun Hypothesis' as proposed by Nisbet (1990, 2002) and Kennett *et al.* (2002) is not responsible for the methane increases at the YD–PB transition period. This non-hydrate source for the methane rise is consistent with the interpretation of Schaefer *et al.* (2006) and Sowers (2006*b*), as well as other lines of evidence (Chappellaz *et al.* 1997; Maslin & Thomas 2003; Maslin *et al.* 2004). It is feasible that a gradual, non-catastrophic, release of *thermogenic* hydrate occurred during segment 3, but not for segments 1 or 2. This release of thermogenic gas could also be conventional natural gas seepage, however, it is not clear why this source would vacillate over relatively short geological time periods.

8. Conclusions

Insights into today's rapid rise in tropospheric methane can be gained by examining analogous increases in the past. The key to this is correctly assessing the magnitude of the methane emission sources and sinks. Stable carbon and hydrogen isotopes of tropospheric methane, as recorded in ice samples, provide a useful constraint on the budget estimations. We are able to incorporate anticipated changes in palaeoenvironmental conditions that translate into changes in the isotope signals of methane precursors, to estimate past global $\delta^{13}CH_4$ and δD-CH_4 values. The overall $\delta^{13}CH_4$ and δD-CH_4 variations are relatively small and require careful analytical precision and accuracy to delineate isotopic changes to the budgets. However, such changes between today and the PIH, YD–PB and LGM are discernable. The most obvious is that the palaeomethane is consistently enriched in ^{13}C- and ^{2}H relative to the Modern by approximately 1 to 5‰ for $\delta^{13}CH_4$ and 9‰ for δD-CH_4. This is a somewhat unexpected result, compared with *a priori* methane budgets that reflect the Modern anthropogenic releases of methane from fossil fuels and biomass burning. These global $\delta^{13}CH_4$–δD-CH_4 constraints enable us to more faithfully reconstruct the methane emission and sink profiles. Our initial goal was not to fully, and perhaps artificially, balance the budgets, rather, we used currently available best estimates of the flux intensities and the isotope signatures of the sources and sinks to compare with the measured values over the Modern, PIH, YD and LGM time periods. Our attempt to balance the LGM budget using reasonable changes to flux intensities and $\delta^{13}CH_4$ and δD-CH_4 values was still unsatisfactory. This points out the discrepancies and uncertainties in atmospheric methane budget calculations and the need for further attention.

Close examination of the relationships between tropospheric methane mixing ratio and temperature reveal strong, but changing correlations for different time periods in the latest Pleistocene. Detailed inspection of the YD $\delta^{13}CH_4$–δD-CH_4 records show a remarkable relationship between them from 12.15 to 11.52 kyr BP. Based on the isotope mass balances, a plausible explanation is the waxing and waning of thermogenic emissions. The tight $\delta^{13}CH_4$–δD-CH_4 relationship appears to breakdown during the YD–PB transition, suggesting that factors

other than thermogenic natural gas are the cause. In both age cases, catastrophic releases of hydrates with Archaeal isotope signatures can be ruled out. Thermogenic clathrate releases are possible for the YD period, but so are conventional natural gas seepages.

We thank Ed Brook for valuable discussions. We also thank Todd Sowers and an anonymous reviewer for very helpful comments. This work was supported by a fellowship from DAAD (German Academic Exchange Service, H.S.), Petroleum Research Fund of the American Chemical Society (H.S.), Canadian Foundation for Climate and Atmospheric Sciences CFCAS MAMMOTH grant (M.J.W.) and NSERC Discovery grant (M.J.W.).

References

Allan, W., Lowe, D. C., Gomez, A. J., Struthers, H. & Brailsford, G. W. 2005 Interannual variation of ^{13}C in tropospheric methane: implications for a possible atomic chlorine sink in the marine boundary layer. *J. Geophys. Res.* **110**, D11306. (doi:11310.11029/12004JD005650)

Alley, R. B. 2000 The Younger Dryas cold interval as viewed from central Greenland. *Quaternary Sci. Rev.* **19**, 213–226. (doi:10.1016/S0277-3791(99)00062-1)

Alley, R. B. 2004 GISP2 ice core temperature and accumulation data. *IGBP PAGES/World Data Center for Paleoclimatology Data Contribution Series No. 2004-013.* NOAA/NGDC Paleoclimatology Program, Boulder CO, USA.

Alperin, M. J., Reeburgh, W. S. & Whiticar, M. J. 1988 Carbon and hydrogen isotope fractionation resulting from anaerobic methane oxidation. *Global Biogeochem. Cycles* **2**, 279–288.

Aselmann, I. & Crutzen, P. J. 1989 Global distribution of natural freshwater wetlands and rice paddies, their net primary productivity, seasonality, and possible methane emissions. *J. Atmos. Chem.* **8**, 307–358. (doi:10.1007/BF00052709)

Bellisario, L. M., Bubier, J. L., Moore, T. R. & Chanton, J. P. 1999 Controls on CH_4 emissions from a northern peatland. *Global Biogeochem. Cycles* **13**, 81–92. (doi:10.1029/1998GB900021)

Bergamaschi, P., Bräunlich, M., Marik, T. & Brenninkmeijer, C. A. M. 2000 Measurements of the carbon and hydrogen isotopes of atmospheric methane at Izaña, Tenerife: seasonal cycles and synoptic-scale variations. *J. Geophys. Res.* **105**, 14 531–14 546. (doi:10.1029/1999JD901176)

Bilek, R. S., Tyler, S. C., Kurihara, M. & Yagi, K. 2001 Investigation of cattle methane production and emission over a 24-hour period using measurements of $\delta^{13}C$ and δD of emitted CH_4 and rumen water. *J. Geophys. Res.* **106**, 15 405–15 413. (doi:10.1029/2001JD900177)

Blair, N. E., Boehme, S. E. & Carter Jr, W. D. 1993 The carbon isotope biogeochemistry of methane production in anoxic sediments: 1. Field observations. In *Biogeochemistry of global change* (ed. R. S. Oremland), pp. 574–593. New York, NY: Chapman & Hall.

Botz, R., Pokojski, H. D., Schmitt, M. & Thomm, M. 1996 Carbon isotope fractionation during bacterial methanogenesis by CO_2 reduction. *Org. Geochem.* **25**, 255–262. (doi:10.1016/S0146-6380(96)00129-5)

Bousquet, P. *et al.* 2006 Contribution of anthropogenic and natural sources to atmospheric methane variability. *Nature* **443**, 439–443. (doi:10.1038/nature05132)

Boutton, T. W., Arshad, M. A. & Tieszen, L. L. 1983 Stable isotope analysis of termite food-habits in east-African grasslands. *Oecologia* **59**, 1–6. (doi:10.1007/BF00388065)

Bowes, H. L. & Hornibrook, E. R. C. 2006 Emission of highly ^{13}C-depleted methane from an upland blanket mire. *Geophys. Res. Lett.* **33**, L04401. (doi:10.1029/2005GL025209)

Boyle, E. A. 1997 Cool tropical temperatures shift the global $\delta^{18}O$–T relationship: an explanation for the ice core $\delta^{18}O$–borehole thermometry conflict? *Geophys. Res. Lett.* **3**, 273–276. (doi:10.1029/97GL00081)

Bréas, O., Guillou, C., Reniero, F. & Wada, F. E. 2001 The global methane cycle: isotopes and mixing ratios, sources and sinks. *Isotopes Environ. Health Stud.* **37**, 257–379.

Brook, E. J., Sowers, T. A. & Orchardo, J. 1996 Rapid variations in atmospheric methane concentration during the past 110,000 years. *Science* **273**, 1087–1091. (doi:10.1126/science.273.5278.1087)

Brook, E. J., Harder, S., Severinghaus, J. P., Steig, E. J. & Sucher, C. M. 2000 On the origin and timing of rapid changes in atmospheric methane during the last glacial period. *Global Biogeochem. Cycles* **14**, 559–572. (doi:10.1029/1999GB001182)

Burke Jr, R. A., Barber, T. R. & Sackett, W. M. 1988 Methane flux and stable hydrogen and carbon isotope composition of sedimentary methane from the Florida Everglades. *Global Biogeochem. Cycles* **2**, 329–340.

Butler, T. M., Simmonds, I. & Rayner, P. J. 2004 Mass balance inverse modelling of methane in the 1990s using a chemistry transport model. *Atmos. Chem. Phys.* **4**, 2561–2580.

Caillon, N., Severinghaus, J. P., Jouzel, J., Barnola, J.-M., Kang, J. & Lipenkov, V. Y. 2003 Timing of atmospheric CO_2 and Antarctic temperature changes across termination III. *Science* **5613**, 1728–1731. (doi:10.1126/science.1078758)

Cantrell, C. A., Shetter, R. E., McDaniel, A. H., Calvert, J. G., Davidson, J. A., Lowe, D. C., Tyler, S. C., Cicerone, R. J. & Greenberg, J. P. 1990 Carbon kinetic isotope effect in the oxidation of methane by the hydroxyl radical. *J. Geophys. Res.* **95**, 22 455–22 462.

Chanton, J. P. 2005 The effect of gas transport on the isotope signature of methane in wetlands. *Org. Geochem.* **36**, 753–768. (doi:10.1016/j.orggeochem.2004.10.007)

Chanton, J. P., Rutkowski, C. M., Schwartz, C. C., Ward, D. E. & Boring, L. 2000 Factors influencing the stable carbon isotopic signature of methane from combustion and biomass burning. *J. Geophys. Res.* **105**, 1867–1877. (doi:10.1029/1999JD900909)

Chappellaz, J. A., Blunier, T., Raynaud, D., Barnola, J. M., Schwander, J. & Stauffer, B. 1993*a* Synchronous changes in atmospheric CH_4 and Greenland climate between 40 and 80 kyr BP. *Nature* **366**, 443–445. (doi:10.1038/366443a0)

Chappellaz, J. A., Fung, I. Y. & Thompson, A. M. 1993*b* The atmospheric CH_4 increase since the Last Glacial Maximum (1). Source estimates. *Tellus B* **45**, 228–241. (doi:10.1034/j.1600-0889.1993.t01-2-00002.x)

Chappellaz, J., Blunier, T., Kints, S., Dällenbach, A., Barnola, J. M., Schwander, J., Raynaud, D. & Stauffer, B. 1997 Changes in the atmospheric CH_4 gradient between Greenland and Antarctica during the Holocene. *J. Geophys. Res. Atmos.* **102**, 15 987–15 997. (doi:10.1029/97JD01017)

Chen, Y.-H. & Prinn, R. G. 2006 Estimation of atmospheric methane emissions between 1996 and 2001 using a three-dimensional global chemical transport model. *J. Geophys. Res.* **111**, D10307. (doi:10.1029/2005JD006058)

Cicerone, R. J. & Oremland, R. S. 1988 Biogeochemical aspects of atmospheric methane. *Global Biogeochem. Cycles* **2**, 299–327.

Collatz, G. J., Berry, J. A. & Clark, J. S. 1998 Effects of climate and atmospheric CO_2 partial pressure on the global distribution of C_4 grasses: present, past, and future. *Oecologia* **114**, 441–454. (doi:10.1007/s004420050468)

Conway, T. J., Tans, P. P., Waterman, L. S., Thoning, K. W., Kitzis, D. R., Massarie, K. A. & Zhang, N. 1994 Evidence for interannual variability of the carbon cycle for the National Oceanic and Atmospheric Administration/Climate Monitoring Diagnostics Laboratory Global Air Sampling Network. *J. Geophys. Res.* **99**, 22 831–22 855. (doi:10.1029/94JD01951)

Craig, H. & Chou, C. C. 1982 Methane: the record in polar ice cores. *Geophys. Res. Lett.* **9**, 1221–1224.

Craig, H., Chou, C. C., Welhan, J. A., Stevens, C. M. & Engelkemeir, A. 1988 The isotopic composition of methane in polar ice cores. *Science* **242**, 1535–1539. (doi:10.1126/science.242.4885.1535)

Cuffey, K. M. & Clow, G. D. 1997 Temperature, accumulation, and ice sheet elevation in central Greenland through the last deglacial transition. *J. Geophys. Res.* **102**, 26 383–26 396. (doi:10.1029/96JC03981)

Cuffey, K. M., Alley, R. B., Grootes, P. M., Bolzan, J. M. & Sridhar, A. 1994 Calibration of the $\delta^{18}O$ isotopic paleothermometer for central Greenland using borehole temperatures. *J. Glaciol.* **40**, 341–349.

Cuffey, K. M., Clow, G. D., Alley, R. B., Stuiver, M., Waddington, E. D. & Saltus, R. W. 1995 Large Arctic temperature change at the Wisconsin–Holocene glacial transition. *Science* **270**, 455–458. (doi:10.1126/science.270.5235.455)

Dällenbach, A., Blunier, T., Flückiger, J., Stauffer, B., Chappellaz, J. & Raynaud, D. 2000 Changes in the atmospheric CH_4 gradient between Greenland and Antarctica during the Last Glacial and the transition to the Holocene. *Geophys. Res. Lett.* **27**, 1005–1008. (doi:10.1029/1999GL010873)

Davidson, J. A., Cantrell, C. A., Tyler, S. C., Calvert, J. G., Cicerone, R. J. & Shetter, R. E. 1986 The carbon kinetic isotope effect in the $CH_4 + OH$ reaction. *EOS* **67**, 245.

Davidson, J. A., Cantrell, C. A., Tyler, S. C., Shetter, R. E., Cicerone, R. J. & Calvert, J. G. 1987 Carbon kinetic isotope effect in the reaction of CH_4 with HO. *J. Geophys. Res.* **92**, 2195–2199.

DeBano, L. F., Neary, D. G. & Ffolliott, P. F. 1998 *Fire effects on ecosystems*, p. 333. New York, NY: J. Wiley and Sons, Ltd.

Dlugokencky, E. J., Steele, L. P., Lang, P. M. & Masarie, K. A. 1994 The growth rate and distribution of atmospheric methane. *J. Geophys. Res.* **99**, 17 021–17 043. (doi:10.1029/94JD01245)

Dlugokencky, E. J., Masarie, K. A., Lang, P. M. & Tans, P. P. 1998 Continuing decline in the growth rate of the atmospheric methane burden. *Nature* **393**, 447–450. (doi:10.1038/30934)

Dlugokencky, E. J., Houweling, S., Bruhwiler, L., Masarie, K. A., Lang, P. M., Miller, J. B. & Tans, P. P. 2003 Atmospheric methane levels off: temporary pause or a new steady-state? *Geophys. Res. Lett.* **30**, 1992. (doi:10.1029/2003GL018126)

Dlugokencky, E. J., Myers, R. C., Lang, P. M., Masarie, K. A., Crotwell, A. M., Thoning, K. W., Hall, B. D., Elkins, J. W. & Steele, L. P. 2005 Conversion of NOAA atmospheric dry air CH_4 mole fractions to a gravimetrically prepared standard scale. *J. Geophys. Res.* **110**, D18306. (doi:10.1029/2005JD006035)

Donner, L. & Ramanathan, V. 1980 Methane and nitrous oxide: their effects on the terrestrial climate. *J. Atmos. Sci.* **37**, 119–124. (doi:10.1175/1520-0469(1980)037<0119:MANOTE>2.0.CO;2)

Ehleringer, J. R. & Monson, R. K. 1993 Evolutionary and ecological aspects of photosynthetic pathway variation. *Annu. Rev. Ecol. Syst.* **24**, 411–439. (doi:10.1146/annurev.es.24.110193.002211)

Ehleringer, J. R., Cerling, T. E. & Helliker, B. R. 1997 C_4 photosynthesis, atmospheric CO_2, and climate. *Oecologia* **112**, 285–299. (doi:10.1007/s004420050311)

Enting, I. G. 2002 *Inverse problems in atmospheric constituent transport*. New York, NY: Cambridge University Press.

Etheridge, D. M., Steele, L. P., Francey, R. J. & Langenfelds, R. L. 1998 Atmospheric methane between 1000 A.D. and present: evidence of anthropogenic emissions and climatic variability. *J. Geophys. Res.* **103**, 15 979–15 993. (doi:10.1029/98JD00923)

Fairbanks, R. G. 1989 A 17,000-year-glacio-eustatic sea level record: influence of glacial melting rates on the Younger Dryas event and deep-ocean circulation. *Nature* **342**, 637–642. (doi:10.1038/342637a0)

Fawcett, P. J., Ágústsdóttir, A. M., Alley, R. B. & Shuman, C. A. 1997 The Younger Dryas termination and North Atlantic deepwater formation: insights from climate model simulations and Greenland ice core data. *Paleoceanography* **12**, 23–38. (doi:10.1029/96PA02711)

Ferretti, D. F. *et al.* 2005 Unexpected changes to the global methane budget over the past 2000 years. *Science* **309**, 1714–1717. (doi:10.1126/science.1115193)

Fey, A., Claus, P. & Conrad, R. 2004 Temporal change of ^{13}C isotopic signatures and methanogenic pathways in rice field soil incubated anoxically at different temperatures. *Geochim. Cosmochim. Acta* **68**, 293–306. (doi:10.1016/S0016-7037(03)00426-5)

Francey, R. F., Allison, C. E., Etheridge, D. M., Trudinger, C. M., Enting, I. G., Leuenberger, M., Langenfelds, R. L., Michel, E. & Steele, L. P. 1999 A 1000-year high precision record of $\delta^{13}C$ in atmospheric CO_2. *Tellus B* **51**, 170–193. (doi:10.1034/j.1600-0889.1999.t01-1-00005.x)

François, L. M., Delire, C., Warnant, P. & Munhoven, G. 1998 Modelling the glacial–interglacial changes in the continental biosphere. *Glob. Planet. Change* **16–17**, 37–52. (doi:10.1016/S0921-8181(98)00005-8)

Frankenberg, C., Meirink, J.-F., van Weele, M., Platt, U. & Wagner, T. 2005 Assessing methane emissions from global space-borne observations. *Science* **308**, 1010–1014. (doi:10.1126/science.1106644)

Frankenberg, C., Meirink, J. F., Bergamaschi, P., Goede, A. P. H., Heimann, M., Körner, S., Platt, U., van Weele, M. & Wagner, T. 2006 Satellite chartography of atmospheric methane from SCIAMACHY on board ENVISAT: analysis of the years 2003 and 2004. *J. Geophys. Res.* **111**, D07303. (doi:10.1029/2005JD006235)

Friedrich, M., Kromer, B., Spurk, M., Hofmann, J. & Kaiser, K. F. 1999 Paleo-environment and radiocarbon calibration as derived from Late Glacial/Early Holocene tree-ring chronologies. *Quatern. Int.* **61**, 27–39.

Fung, I., John, J., Lerner, J., Matthews, E., Prather, M., Steele, L. P. & Fraser, P. J. 1991 Three-dimensional model synthesis of the global methane cycle. *J. Geophys. Res.* **96**, 13 033–13 065.

Grachev, A. M. & Severinghaus, J. P. 2005 A revised $+10\pm4$°C magnitude of the abrupt change in Greenland temperature at the Younger Dryas termination using published GISP2 gas isotope data and air thermal diffusion constants. *Quaternary Sci. Rev.* **24**, 513–519. (doi:10.1016/j.quascirev.2004.10.016)

Gordon, S. & Mulac, W. A. 1975 Reaction of the OH ($X2\pi$) radical produced by the pulse radiolysis of water vapour. In *Proc. Symp. on Chemical Kinetics Data for the Upper and Lower Atmosphere. Int. J. Chem. Kinetics Symp.* **1**, 289–299.

Gröcke, D. R. 2002 The carbon isotope composition of ancient CO_2 based on higher-plant organic matter. *Phil. Trans. R. Soc. A* **360**, 633–658. (doi:10.1098/rsta.2001.0965)

Grootes, P. M. & Stuiver, M. 1997 Oxygen 18/16 variability in Greenland snow and ice with 10^3 to 10^5-year time resolution. *J. Geophys. Res.* **102**, 26 455–26 470. (doi:10.1029/97JC00880)

Grootes, P. M., Stuiver, M., White, J. W. C., Johnsen, S. J. & Jouzel, J. 1993 Comparison of oxygen isotope records from the GISP2 and GRIP Greenland ice cores. *Nature* **366**, 552–554. (doi:10.1038/366552a0)

Haberle, S. G. & Ledru, M.-P. 2001 Correlations of char coal records of fires from the past 16,000 years in Indonesia, Papua New Guinea, and Central and South America. *Quaternary Res.* **55**, 97–104. (doi:10.1006/qres.2000.2188)

Hao, W. M. & Ward, D. E. 1993 Methane production from global biomass burning. *J. Geophys. Res.* **98**, 20 657–20 661.

Hein, R., Crutzen, P. J. & Heimann, M. 1997 An inverse modeling approach to investigate the global atmospheric methane cycle. *Global Biogeochem. Cycles* **11**, 43–76. (doi:10.1029/96GB03043)

Hornibrook, E. R. C., Longstaffe, F. J. & Fyfe, W. S. 1997 Spatial distribution of microbial methane production pathways in temperate zone wetland soils: stable carbon and hydrogen isotope evidence. *Geochim. Cosmochim. Acta* **61**, 745–753. (doi:10.1016/S0016-7037(96)00368-7)

Houghton, J. T., Jenkins, G. J. & Ephraums, J. J. (eds) 1990. *Climate change: the IPC scientific assessment*, p. 337. Cambridge, UK: Cambridge University Press.

Houweling, S., Dentener, F. & Lelieveld, J. 2000 Simulation of preindustrial atmospheric methane to constrain the global source strength of natural wetlands. *J. Geophys. Res.* **105**, 17 243–17 255. (doi:10.1029/2000JD900193)

Houweling, S., Röckmann, T., Aben, I., Keppler, F., Krol, M., Meirink, J. F., Dlugokencky, E. & Frankenberg, C. 2006 Atmospheric constraints on global emissions of methane from plants. *Geophys. Res. Lett.* **33**, L15821. (doi:10.1029/2006GL026162)

Huber, C., Leuenberger, M., Spahni, R., Flückiger, J., Schwander, J., Stocker, T. F., Johnsen, S., Landais, A. & Jouzel, J. 2006 Isotope calibrated Greenland temperature record over Marine Isotope Stage 3 and its relation to CH_4. *Earth Planet. Sci. Lett.* **243**, 504–519. (doi:10.1016/j.epsl.2006.01.002)

Hughen, K. A., Eglinton, T. I., Xu, L. & Makou, M. 2004 Abrupt tropical vegetation response to rapid climate changes. *Science* **304**, 1955–1959. (doi:10.1126/science.1092995)

Jain, A. K., Briegleb, B. P., Minschwaner, K. & Wuebbles, D. J. 2000 Radiative forcings and global warming potentials of 39 greenhouse gases. *J. Geophys. Res.* **105**, 20 773–20 790. (doi:10.1029/2000JD900241)

Johnsen, S. J., Dansgaard, W. W. & White, J. W. C. 1989 The origin of Arctic precipitation under present and glacial conditions. *Tellus B* **41**, 452–468.

Johnsen, S. J., Dahl-Jensen, D., Dansgaard, W. & Gundestrup, N. 1995 Greenland paleotemperatures derived from GRIP bore hole temperature and ice core isotope profiles. *Tellus B* **47**, 624–629. (doi:10.1034/j.1600-0889.47.issue5.9.x)

Jouzel, J. *et al.* 1997 Validity of the temperature reconstruction from water isotopes in ice cores. *J. Geophys. Res.* **102**, 26 471–26 487. (doi:10.1029/97JC01283)

Kaplan, J. O. 2002 Wetlands at the Last Glacial Maximum: distribution and methane emissions. *Geophys. Res. Lett.* **29**, 1079. (doi:10.1029/2001GL013366)

Kaplan, J. O., Folberth, G. & Hauglustaine, D. A. 2004 Ice age methane revisited: oceans, lightning, and the steady wetland source. *EOS Trans. AGU Joint Assembly Supp.* **85**, GC21A–18.

Kaplan, J. O., Folberth, G. & Hauglustaine, D. A. 2006 Role of methane and biogenic volatile organic compound sources in late glacial and Holocene fluctuations of atmospheric methane concentrations. *Global Biogeochem. Cycles* **20**, GB2016. (doi:10.1029/2005GB002590)

Keeling, C. D. & Whorf, T. P. 2005 Atmospheric CO_2 records from sites in the SIO air sampling network. In *Trends: a compendium of data on global change*. Carbon Dioxide Information Analysis Center, Oak Ridge National Laboratory. U.S. Department of Energy, Oak Ridge, TN, USA.

Kennett, J. P., Cannariato, K. G., Hendy, I. L. & Behl, R. J. 2002 *Methane hydrates in quaternary climate change: the clathrate gun hypothesis*. Washington, DC: American Geophysical Union.

Keppler, F., Hamilton, J. T. G., Braß, M. & Röckmann, T. 2006 Methane emissions from terrestrial plants under aerobic conditions. *Nature* **439**, 187–191. (doi:10.1038/nature04420)

King, S. L., Quay, P. D. & Lansdowne, J. M. 1989 The $^{13}C/^{12}C$ kinetic isotope effect for soil oxidation of methane at ambient atmospheric concentrations. *J. Geophys. Res.* **94**, 18 273–18 277.

Krinner, G., Genthon, C. & Jouzel, J. 1997 GCM analysis of local influences on ice core signals. *Geophys. Res. Lett.* **24**, 2825–2828. (doi:10.1029/97GL52891)

Lang, C., Leuenberger, M., Schwander, J. & Johnsen, S. 1999 16°C rapid temperature variation in central Greenland 70,000 years ago. *Science* **286**, 934–937. (doi:10.1126/science.286.5441.934)

Lassey, K. R., Lowe, D. C. & Manning, M. R. 2000 The trend in atmospheric methane δC and implications for isotopic constraints on the global methane budget. *Global Biogeochem. Cycles* **14**, 41–49. (doi:10.1029/1999GB900094)

Law, R. M. & Vohralik, P. F. 2001 *Methane sources from mass balance inversions: sensitivity to transport*, Tech. Rep. 50, CSIRO Atmos. Res., Aspendale, Victoria, Australia.

Lelieveld, J., Crutzen, P. J. & Dentener, F. S. 1998 Changing concentration, lifetime, and climate forcing of atmospheric methane. *Tellus B* **50**, 128–150. (doi:10.1034/j.1600-0889.1998.t01-1-00002.x)

Levin, I., Bergamaschi, P., Dörr, H. & Trapp, D. 1993 Stable isotopic signature of methane from major sources in Germany. *Chemosphere* **26**, 161–177. (doi:10.1016/0045-6535(93)90419-6)

Luyendyk, B., Kennett, J. & Clark, J. F. 2005 Hypothesis for increased atmospheric methane input from hydrocarbon seeps on exposed continental shelves during glacial low sea level. *Mar. Petrol. Geol.* **22**, 591–596. (doi:10.1016/j.marpetgeo.2004.08.005)

Marino, B. D., McElroy, M. B., Salawitch, R. J. & Spaulding, G. W. 1992 Glacial-to-interglacial variations in the carbon isotopic composition of atmospheric CO_2. *Nature* **357**, 461–466. (doi:10.1038/357461a0)

Martinerie, P., Brasseur, G. P. & Granier, C. 1995 The chemical composition of ancient atmospheres: a model study constrained by ice core data. *J. Geophys. Res.* **100**, 14 291–14 304. (doi:10.1029/95JD00826)

Maslin, M. A. & Thomas, E. 2003 Balancing the deglacial global carbon budget: the hydrate factor. *Quaternary Sci. Rev.* **22**, 1729–1736. (doi:10.1016/S0277-3791(03)00135-5)

Maslin, M., Owen, M., Day, S. & Long, D. 2004 Linking continental-slope failures and climate change: testing the clathrate gun hypothesis. *Geology* **32**, 53–56. (doi:10.1130/G20114.1)

Masson-Delmotte, V., Jouzel, J., Landais, A., Stievenard, M., Johnsen, S. J., White, J. W. C., Werner, M., Sveinbjornsdottir, A. & Fuhrer, K. 2005 GRIP deuterium excess reveals rapid and orbital-scale changes in Greenland moisture origin. *Science* **309**, 118–121. (doi:10.1126/science.1108575)

Matthews, E. & Fung, I. 1987 Methane emissions from natural wetlands: global distribution, area, and environmental characteristics of sources. *Global Biogeochem. Cycles* **1**, 61–86.

McCarthy, M. C., Connell, P. & Boering, K. A. 2001 Isotopic fractionation of methane in the stratosphere and its effect on free tropospheric isotopic compositions. *Geophys. Res. Lett.* **28**, 3657–3660. (doi:10.1029/2001GL013159)

Meese, D. A. *et al.* 1994 Preliminary depth-age scale of the GISP2 ice core. *Special CRREL Report 94-1*, USA.

Metges, C., Kempe, K. & Schmidt, H. L. 1990 Dependence of the carbon-isotope contents of breath carbon dioxide, milk, serum, and rumen fermentation products on the $\delta^{13}C$ value of food in dairy cows. *Br. J. Nutrit.* **63**, 187–196. (doi:10.1079/BJN19900106)

Michalak, A. M., Hirsch, A., Bruhwiler, L., Gurney, K. R., Peters, W. & Tans, P. P. 2005 Maximum likelihood estimation of covariance parameters for Bayesian atmospheric trace gas surface flux inversions. *J. Geophys. Res.* **110**, D24107. (doi:10.1029/2005JD005970)

Michelsen, H. A. & Simpson, W. R. 2001 Relating state-dependent cross sections to non-Arrhenius behavior for the $Cl+CH_4$ reaction. *J. Phys. Chem. A* **105**, 1476–1488. (doi:10.1021/jp0016784)

Miller, J. B., Mack, K. A., Dissly, R., White, J. W. C., Dlugokencky, E. J. & Tans, P. P. 2002 Development of analytical methods and measurements of $^{13}C/^{12}C$ in atmospheric CH_4 from the NOAA Climate Monitoring and Diagnostics Laboratory Global Air Sampling Network. *J. Geophys. Res.* **107**, 4178. (doi:10.1029/2001JD000630)

Minschwaner, K., Carver, R. W., Briegleb, B. P. & Roche, A. E. 1998 Infrared radiative forcing and atmospheric lifetimes of trace species based on observations from UARS. *J. Geophys. Res.* **103**, 23 243–23 253. (doi:10.1029/98JD02116)

Nisbet, E. G. 1990 The end of the ice age. *Can. J. Earth Sci.* **27**, 48–157.

Nisbet, E. G. 2002 Have sudden large releases of methane from geological reservoirs occurred since the Last Glacial Maximum, and could such releases occur again? *Phil. Trans. R. Soc. A* **360**, 581–607. (doi:10.1098/rsta.2001.0958)

Paterson, W. S. B. 1994 *The physics of glaciers*, p. 480, 3rd edn. Oxford, UK: Pergamon.

Petit, J. *et al.* 1999 Climate and atmospheric history of the past 420,000 years from the Vostok ice core, Antarctica. *Nature* **399**, 429–436. (doi:10.1038/20859)

Petrenko, V. V., Severinghaus, J. P., Brook, E. J., Reeh, N. & Schaefer, H. 2006 Gas records from the West Greenland ice margin covering the Last Glacial Termination: a horizontal ice core. *Quaternary Sci. Rev.* **25**, 865–875. (doi:10.1016/j.quascirev.2005.09.005)

Prather, M. *et al.* 2001 Atmospheric chemistry and greenhouse gases. In *Climate change 2001: the scientific basis* (eds J. T. Houghton, Y. Ding, D. J. Griggs, M. Noguer, P. J. van der Linden, X. Dai, K. Maskell & C. A. Johnson), pp. 239–288. Cambridge, UK: IPCC Cambridge University Press.

Prentice, I. C., Sykes, M. T., Lautenschlager, M., Harrison, S. P., Denissenko, O. & Bartlein, P. J. 1993 Modelling global vegetation patterns and terrestrial carbon storage at the Last Glacial Maximum. *Global Ecol. Biogeogr. Lett.* **3**, 67–76. (doi:10.2307/2997548)

Quay, P., Stutsman, J., Wilbur, D., Snover, A., Dlugokencky, E. & Brown, T. 1999 The isotopic composition of atmospheric methane. *Global Biogeochem. Cycles* **13**, 445–462. (doi:10.1029/1998GB900006)

Quay, P. D. *et al.* 1991 Carbon isotopic composition of atmospheric CH_4: fossil and biomass burning source strengths. *Global Biogeochem. Cycles* **5**, 25–47.

Reeburgh, W. S., Hirsch, A. I., Sansone, F. J., Popp, B. N. & Rust, T. M. 1997 Carbon kinetic isotope effect accompanying microbial oxidation of methane in boreal forest soils. *Geochim. Cosmochim. Acta* **61**, 4761–4767. (doi:10.1016/S0016-7037(97)00277-9)

Rice, A. L., Tyler, S. C., McCarthy, M. C., Boering, K. A. & Atlas, E. 2003 Carbon and hydrogen isotopic compositions of stratospheric methane: 1. High-precision observations from the NASA ER-2 aircraft. *J. Geophys. Res.* **108**, 4460. (doi:10.1029/2002JD003042)

Ridgwell, A. J., Marshall, S. J. & Gregson, K. 1999 Consumption of atmospheric methane by soils: a process-based model. *Global Biogeochem. Cycles* **13**, 59–70. (doi:10.1029/1998GB900004)

Rust, F. E. 1981 $\delta(^{13}C/^{12}C)$ of ruminant methane and its relationship to atmospheric methane. *Science* **211**, 1044–1046. (doi:10.1126/science.7466376)

Saueressig, G., Bergamaschi, P., Crowley, J. N., Fischer, H. & Harris, G. W. 1995 Carbon kinetic isotope effect in the reaction of CH_4 with Cl atoms. *Geophys. Res. Lett.* **22**, 1225–1228. (doi:10.1029/95GL00881)

Saueressig, G., Crowley, J. N., Bergamaschi, P., Bruehl, C., Brenninkmeijer, C. A. & Fischer, H. 2001 Carbon 13 and D kinetic isotope effects in the reactions of CH_4 with $O(^1D)$ and OH: new laboratory measurements and their implications for the isotopic composition of stratospheric methane. *J. Geophys. Res.* **106**, 23 127–23 138. (doi:10.1029/2000JD000120)

Schaefer, H. 2005 Stable carbon isotopic composition of methane from ancient ice samples, p. 191. PhD thesis, University of Victoria.

Schaefer, H. & Whiticar, M. J. 2007 Measurement of stable carbon isotope ratios of methane in ice samples. *Org. Geochem.* **38**, 216–226. (doi:10.1016/j.orggeochem.2006.10.006)

Schaefer, H. & Whiticar, M. J. In press. Potential glacial–interglacial changes in stable carbon isotope ratios of methane sources and sink fractionation. *Global Biogeochem. Cycles*.

Schaefer, H., Whiticar, M. J., Brook, E. J., Petrenko, V. V., Ferretti, D. F. & Severinghaus, J. P. 2006 Ice record of $\delta^{13}C$ for atmospheric CH_4 across the Younger Dryas–Preboreal transition. *Science* **313**, 1109–1112. (doi:10.1126/science.1126562)

Schulze, E., Lohmeyer, S. & Giese, W. 1998 Determination of $^{13}C/^{12}C$-ratios in rumen produced methane and CO_2 of cows, sheep and camels. *Isotopes Environ. Health Stud.* **34**, 75–79.

Schwander, J., Sowers, T., Barnola, J.-M., Blunier, T., Malaizé, B. & Fuchs, T. 1997 Age scale of the air in the summit ice: implication for glacial–interglacial temperature change. *J. Geophys. Res.* **102**, 19 483–19 494. (doi:10.1029/97JD01309)

Severinghaus, J. P. & Brook, E. J. 1999 Abrupt climate change at the end of the Last Glacial period inferred from trapped air in polar ice. *Science* **286**, 930–933. (doi:10.1126/science.286.5441.930)

Severinghaus, J. P., Sowers, T., Brook, E. J., Alley, R. B. & Bender, M. L. 1998 Timing of abrupt climate change at the end of the Younger Dryas interval from thermally fractionated gases in polar ice. *Nature* **341**, 141–146. (doi:10.1038/34346)

Smith, H. J., Fischer, H., Wahlen, M., Mastroianni, D. & Deck, B. 1999 Dual modes of the carbon cycle since the Last Glacial Maximum. *Nature* **400**, 248–250. (doi:10.1038/22291)

Snover, A. K. & Quay, P. D. 2000 Hydrogen and carbon kinetic isotope effects during soil uptake of atmospheric methane. *Global Biogeochem. Cycles* **14**, 25–39. (doi:10.1029/1999GB900089)

Snover, A. K., Quay, P. D. & Hao, W. M. 2000 The D/H content of methane emitted from biomass burning. *Global Biogeochem. Cycles* **14**, 11–24. (doi:10.1029/1999GB900075)

Sowers, T. A. 2006*a* Methane isotope records spanning the last 160 kyr: correlations and conundrums. *EOS Trans. AGU Fall Meet. Suppl.*, **87**, Abstract 1094.

Sowers, T. A. 2006*b* Late Quaternary atmospheric CH_4 isotope record suggests marine clathrates are stable. *Science* **311**, 838–840. (doi:10.1126/science.1121235)

Sowers, T. A. & Bender, M. 1995 Climate records during the last deglaciation. *Science* **269**, 210–214. (doi:10.1126/science.269.5221.210)

Sowers, T. A., Bernard, S., Aballain, O., Chappellaz, J. A., Barnola, J.-M. & Marik, T. 2005 Records of the $\delta^{13}C$ of atmospheric CH_4 over the last 2 centuries as recorded in Antarctic snow and ice. *Global Biogeochem. Cycles* **19**, GB2002. (doi:10.1029/2004GB002408)

Spahni, R. *et al.* 2005 Atmospheric methane and nitrous oxide of the late Pleistocene from Antarctic ice cores. *Science* **310**, 1317–1321. (doi:10.1126/science.1120132)

Staffelbach, T., Neftel, A., Stauffer, B. & Jacob, D. 1991 A record of the atmospheric methane sink from formaldehyde in polar ice cores. *Nature* **349**, 603–605. (doi:10.1038/349603a0)

Stauffer, B., Flückiger, J., Monnin, E., Schwander, J., Barnola, J.-C. & Chappellaz, J. 2002 Atmospheric CO_2, CH_4 and NO_2 records over the past 60,000 years based on the comparison of different polar ice cores. *Ann. Glaciol.* **35**, 202–208.

Steig, E. J., Grootes, P. M. & Stuiver, M. 1994 Seasonal precipitation timing and ice core records. *Science* **266**, 1885–1886. (doi:10.1126/science.266.5192.1885)

Steudler, P. M., Melillo, J. M., Feigl, B. J., Neill, C., Piccolo, M. C. & Cerri, C. C. 1996 Consequence of forest-to-pasture conversion on CH_4 fluxes in the Brazilian Amazon Basin. *J. Geophys. Res.* **101**, 18 547–18 554. (doi:510.1029/1096JD01551)

Stevens, C. M. & Engelkemeir, A. 1988 Stable carbon isotopic composition of methane from natural and anthropogenic sources. *J. Geophys. Res.* **93**, 725–733.

Stuiver, M., Grootes, P. M. & Braziunas, T. F. 1995 The GISP2 ^{18}O climate record of the past 16,500 years and the role of the sun, ocean and volcanoes. *Quaternary Res.* **44**, 341–354. (doi:10.1006/qres.1995.1079)

Sugimoto, A. & Wada, E. 1995 Hydrogen isotopic composition of bacterial methane: CO_2/H_2 reduction and acetate fermentation. *Geochim. Cosmochim. Acta* **59**, 1329–1337. (doi:10.1016/0016-7037(95)00047-4)

Sugimoto, A., Inoue, T., Kirtibutr, N. & Abe, T. 1998 Methane oxidation by termite mounds estimated by the carbon isotopic composition of methane. *Global Biogeochem. Cycles* **12**, 595–605. (doi:10.1029/98GB02266)

Tans, P. P. 1997 A note on isotopic ratios and the global atmospheric methane budget. *Global Biogeochem. Cycles* **11**, 77–82. (doi:10.1029/96GB03940)

Tayasu, I. 1998 Use of carbon and nitrogen isotope ratios in termite research. *Ecol. Res.* **13**, 377–387. (doi:10.1046/j.1440-1703.1998.00268.x)

Tyler, S. C., Zimmerman, P. R., Cumberbatch, C., Greenberg, J. P., Westberg, C. & Darlington, J. P. E. C. 1988 Measurements and interpretation of $\delta^{13}C$ of methane from termites, rice paddies, and wetlands in Kenya. *Global Biogeochem. Cycles* **2**, 341–355.

Tyler, S. C., Crill, P. M. & Brailsford, G. W. 1994 $^{13}C/^{12}C$ fractionation of methane during oxidation in a temperate forested soil. *Geochim. Cosmochim. Acta* **58**, 1625–1633. (doi:10.1016/0016-7037(94)90564-9)

Tyler, S. C., Ajie, H. O., Rice, A. L., Cicerone, R. J. & Tuazon, E. C. 2000 Experimentally determined kinetic isotope effects in the reaction of CH_4 with Cl: implications for atmospheric CH_4. *Geophys. Res. Lett.* **27**, 1715–1718. (doi:10.1029/1999GL011168)

Valdes, P. J., Beerling, D. J. & Johnson, C. E. 2005 The ice age methane budget. *Geophys. Res. Lett.* **32**, L02704. (doi:10.1029/2004GL021004)

Waldron, S., Fallick, A. E., Lansdown, J. M., Scott, E. M. & Hall, A. J. 1999 The global influence of the hydrogen isotope composition of water on that of bacteriogenic methane from shallow freshwater environments. *Geochim. Cosmochim. Acta* **63**, 2237–2245. (doi:10.1016/S0016-7037(99)00192-1)

Walter, B. P. & Heimann, M. 2000 A process-based, climate-sensitive model to derive methane emissions from natural wetlands: application to five wetland sites, sensitivity to model parameters, and climate. *Global Biogeochem. Cycles* **14**, 745–765. (doi:10.1029/1999GB001204)

Wang, Y. J., Cheng, H., Edwards, R. L., An, Z. S., Wu, J. Y., Shen, C.-C. & Dorale, J. A. 2001 A high-resolution absolute-dated Late Pleistocene monsoon record from Hulu Cave, China. *Science* **294**, 2345–2348. (doi:10.1126/science.1064618)

Wang, J. S., McElroy, M. B., Spivakovsky, C. M. & Jones, D. B. A. 2002 On the contribution of anthropogenic Cl to the increase in $\delta^{13}C$ of atmospheric methane. *Global Biogeochem. Cycles* **16**, 1047. (doi:10.1029/2001GB001572)

Werner, M., Heimann, M. & Hoffmann, G. 2001 Isotopic composition and origin of polar precipitation in present and glacial climate simulations. *Tellus B* **53**, 53–71. (doi:10.1034/j.1600-0889.2001.01154.x)

Whalen, M. N. 1993 The global methane cycle. *Annu. Rev. Earth Planet. Sci.* **21**, 407–426. (doi:10.1146/annurev.ea.21.050193.002203)

Whalen, M., Tanaka, N., Deck, B., Henry, R., Shemesh, A., Fairbanks, R. & Broecker, W. 1990 δD in CH_4: additional constraints for a global CH_4 budget. *EOS Trans. AGU* **71**, 1249.

White, J. W. C., Ciais, P., Figge, R. A., Kenny, R. & Markgraf, V. 1994 A high-resolution record of atmospheric CO_2 content from carbon isotopes in pet. *Nature* **367**, 153–156. (doi:10.1038/367153a0)

Whiticar, M. J. 1990 A geochemical perspective of natural gas and atmospheric methane. *Org. Geochem.* **16**, 531–547. (doi:10.1016/0146-6380(90)90068-B)

Whiticar, M. J. 1993 Stable isotopes and global budgets. In *Atmospheric methane: sources, sinks, and role in global change*, vol. 13 (ed. M. A. K. Khalil). NATO ASI series I, global environmental change, ch. 8, pp. 138–167. New York, NY: Springer.

Whiticar, M. J. 1994 Correlation of natural gases with their sources. In *The petroleum system—from source to trap* (eds L. B. Magoon & W. G. Dow). *AAPG Memoir* **60**, 261–283.

Whiticar, M. J. 1999 Carbon and hydrogen isotope systematics of bacterial formation and oxidation of methane. *Chem. Geol.* **161**, 291–314. (doi:10.1016/S0009-2541(99)00092-3)

Whiticar, M. J. & Faber, E. 1986 Methane oxidation in sediment and water column environments—isotopic evidence. *Org. Geochem.* **10**, 759–768. (doi:10.1016/S0146-6380(86)80013-4)

Whiticar, M. J., Faber, E. & Schoell, M. 1986 Biogenic methane formation in marine and freshwater environments: CO_2 reduction vs. acetate fermentation-isotopic evidence. *Geochim. Cosmochim. Acta* **50**, 693–709. (doi:10.1016/0016-7037(86)90346-7)

Wright, H. A. & Bailey, A. W. 1982 *Fire ecology, United States and southern Canada*, p. 501. New York, NY: J. Wiley and Sons, Ltd.

Wunsch, C. 2006 Abrupt climate change: an alternative view. *Quaternary Res.* **65**, 191–203. (doi:10.1016/j.yqres.2005.10.006)

Yamada, K., Ozaki, Y., Nakagawa, F., Sudo, S., Tsuruta, H. & Yoshida, N. 2006 Hydrogen and carbon isotopic measurements of methane from agricultural combustion: implications for isotopic signatures of global biomass burning sources. *J. Geophys. Res.* **111**, D16306. (doi:10.1029/2005JD006750)

Zimmerman, P. R., Greenberg, J. P., Wandiga, S. O. & Crutzen, P. J. 1982 Termites, a potentially large source of atmospheric methane, carbon dioxide, and molecular hydrogen. *Science* **218**, 563–565. (doi:10.1126/science.218.4572.563)